https://doi.org/10.5194/egusphere-2026-3368
Preprint. Discussion started: 29 June 2026

Enhancing the advection module performance in the EPICC-Model V1.6.0 via GPU-HADVPPM4HIP V1.0 coupling and GPU-optimized strategies

Kai Cao[1], Qizhong Wu[2], Xiao Tang[1,3], Jinxi Li[1], Xueshun Chen[1,3], Huansheng Chen[1], Wending Wang[1], Huangjian Wu[1], Lei Kong[1], Jie Li[1,3], Jiang Zhu[1,3], and Zifa Wang[1,3]

[1]State Key Laboratory of Atmospheric Environment and Extreme Meteorology, Institute of Atmospheric Physics, Chinese Academy of Sciences, Beijing 100029, China

[2]College of Global Change and Earth System Science, Faculty of Geographical Science, Beijing Normal University, Beijing 100875, China

[3]College of Earth and Planetary Sciences, University of Chinese Academy of Sciences, Beijing, 100049, China

Correspondence to: Qizhong Wu (wqizhong@bnu.edu.cn); Xiao Tang (tangxiao@mail.iap.ac.cn)

Abstract

The rapid development of Graphics Processing Units (GPUs) has established new computational paradigms for enhancing air quality modeling efficiency. In this study, the heterogeneous-compute interface for portability (HIP) was implemented to parallel computing of the piecewise parabolic method (PPM) advection solver (HADVPPM) on China's domestic GPU-like accelerators (GPU-like), resulting in a GPU-accelerated version denoted as GPU-HADVPPM4HIP V1.0. Computational performance was enhanced through three strategic optimizations: reducing the central processing unit (CPU) and GPU (CPU-GPU) data transfer frequency, thread-block coordinated indexing, and the Message Passing Interface (MPI) and HIP ("MPI+HIP") hybrid parallelization across heterogeneous computing clusters. Following validation of the GPU-HADVPPM4HIP V1.0 program's offline computational consistency and the pollutant simulation performance of the Emission and atmospheric Processes Integrated and Coupled Community version 1.6.0 (EPICC-Model V1.6.0) on the Earth System Numerical Simulation

https://doi.org/10.5194/egusphere-2026-3368
Preprint. Discussion started: 29 June 2026

Facility (EarthLab), comprehensive performance testing was conducted. Offline benchmark results demonstrated that GPU-HADVPPM4HIP V1.0 achieved a maximum speedup of 556.5x on a GPU-like using the compiler optimization option compared to the Fortran HADVPPM baseline compiled option for a data size of 10^8. Integrating GPU-HADVPPM4HIP V1.0 into EPICC-Model V1.6.0 yielded three distinct versions: the initial HIP-based version (HIP-Ori), a version optimized for CPU and GPU communication frequency (HIP-Opt1), and a further-optimized version employing a thread-block coordinated indexing strategy (HIP-Opt2). Compared to the HIP-Ori version, HIP-Opt1 achieved a model-level computational efficiency improvement of 17.0x. Building upon HIP-Opt1, HIP-Opt2 delivered an additional 1.5x enhancement in computational efficiency. At the module level, including CPU and GPU data transfer overhead, the GPU implementation improves computational efficiency of the advection module by 39.3%; when communication cost is excluded, the advection module attains a 20.5× acceleration relative to its CPU counterpart. This coupling establishes a foundational framework for adapting air quality models to GPU-like architectures and identifies critical optimization pathways. Moreover, the methodology provides essential technical support for achieving full-model GPU implementation of the EPICC-Model, addressing both current computational constraints and future demands for high-resolution air quality simulations.

1. Introduction

Air pollution, a source of fine particulate matter in both urban and rural areas, is associated with an elevated risk of strokes, heart diseases, lung cancer, and acute and chronic respiratory diseases (Atkinson et al., 2010; Kim et al., 2015; Liu et al., 2016; Milton and White, 2020). The air quality forecasting system centered on the air quality model plays a critical role in the timely dissemination of forecasting alerts and early warning information to the public. The accuracy of air quality forecasting is jointly constrained by the spatial resolution of input datasets, including emission inventories, terrain, and meteorological parameters (Gupta et al., 2015; Georgiou et al., 2022). High-resolution model configurations have demonstrated improvements in the accuracy of air quality forecasting (Georgiou et al., 2018; Podrascanin et al., 2019; Adani et al., 2022; Gao and Zhou, 2024). However, current operational forecasting systems predominantly employ horizontal resolutions ranging from several to tens of kilometers (Wu et al., 2014; Guevara et al., 2021; Tang

https://doi.org/10.5194/egusphere-2026-3368
Preprint. Discussion started: 29 June 2026

et al., 2022; Gao and Zhou, 2024), which inadequately address the requirements for urban-scale high-resolution forecasting and precision management.

Computational demands emerge as a critical limiting factor for high-resolution air quality modeling. On the one hand, doubling the horizontal resolution quadruples the number of computational grids. On the other hand, maintaining numerical integration stability necessitates proportional reduction in temporal integration steps (Georgiou et al., 2022). These combined effects result in exponential growth of computational workload with increasing resolution. It is estimated that when the horizontal resolution of the air quality model is increased by 18 times, the computational load of the model increases by 300 times (Thompson and Selin 2012).

Enhancement of computational efficiency in air quality modeling has been predominantly achieved through hardware-based acceleration strategies. Wang et al. (2017) ported the Global Nested Air Quality Prediction Modeling System (GNAQPMS) to the second-generation Intel Xeon Phi processor (KNL), achieving a 3.5x computational acceleration via MPI and OpenMP hybrid parallelization, vectorization optimization, memory access pattern refinement, thread-local storage reduction, and global communication optimization. The gas-phase chemistry module is widely recognized as the dominant computational bottleneck in air quality models, typically accounting for over 40% of total simulation time (Elbern, 1997; Linford et al., 2011; Wang et al., 2017; Cao et al., 2023). To address this limitation, Wang et al. (2019) developed the MP CBM-Z mechanism by implementing vectorized computation techniques within the CBM-Z framework. Leveraging Single Instruction Multiple Data (SIMD) architecture, their approach enabled multi-point parallel computation for gas-phase chemistry, achieving a 4.9x acceleration in the chemistry module and a 2.22x overall speedup for the entire NAQPMS model when deployed on Intel Xeon Gold 6132 CPUs.

In recent years, GPUs have emerged as transformative accelerators in artificial intelligence and high-performance computing, driven by their massive parallel computing capabilities. In December 2024, the 64th TOP500 list of supercomputers revealed that the El Capitan system has achieved the top spot, becoming the third exascale computing system following Frontier and Aurora, with an HPL score of 1.742 EFLOP/s (Top500, 2024). This computational supremacy primarily originates from its AMD Instinct MI300A GPU accelerators, each containing 14,592 stream processors and

https://doi.org/10.5194/egusphere-2026-3368
Preprint. Discussion started: 29 June 2026

delivering a double-precision floating-point performance of 61.3 TFLOP/s. Remarkably, the computational efficiency of a single MI300A GPU exceeds 1.8 times the peak performance of the Earth-Simulator supercomputer (CPU-based architecture) in Japan, which is Top1 supercomputer in 2003.

The formidable computational capacity of GPUs has opened new directions for enhancing the computational efficiency of air quality models. Alvanos and Christoudias (2017) developed a software package for the global atmospheric chemistry model ECHAM/MESSy Atmospheric Chemistry (EMAC), enabling automated generates CUDA kernels to numerically integrate atmospheric chemical kinetics by the Kinetic PreProcessor (KPP, Damian et al., 2002). Subsequent memory optimization and thread management strategies achieved a 20.4x acceleration for the chemistry module on NVIDIA P100 GPUs. In parallel efforts, Sun et al. (2018) implemented CUDA-based optimization for the second-order Rosenbrock chemical solver (Sandu et al., 1997) within the CAM4-Chem global chemistry-climate model. Through strategic enhancements in fully interleaved memory layout, CUDA streams, and constant memory, they achieved an 11.7x speedup for computation alone and a 3.8x speedup when the data transfer between the CPU and GPU is considered on the NVIDIA Tesla K20X GPU. Notably, Quevedo et al. (2025) adapted the third-order Rosenbrock solver in the CMAQ model by converting Fortran code to CUDA Fortran, evaluating its performance across three chemical mechanisms: RACM2, CB6R5, and SAPRC07. Comparative analysis revealed 51%, 50%, and 35% computational efficiency gains on NVIDIA RTX 2080 Ti GPUs, respectively, while maintaining numerical consistency with CPU-based benchmarks. Through code refactoring from Fortran to standard C and the HIP programming technology, Cao et al. (2025) successfully parallelized the fourth-order Rosenbrock solver on GPU-like architecture. Concurrently, the total model elapsed time was reduced by 46.9%. Regarding another hotspot module in air quality models-the advection module, Cao et al. (2023, 2024) implemented GPU-accelerated adaptations of the CAMx model's advection module using CUDA and HIP heterogeneous technologies, respectively, and the optimized advection module achieved maximum speedups of 80.2x on NVIDIA Tesla V100 GPUs and 28.9x on GPU-like.

Following Cao et al.'s (2025) successful implementation of parallel computing for the gas-phase chemistry module in the EPICC-Model on GPU-like accelerators, the computational time

https://doi.org/10.5194/egusphere-2026-3368
Preprint. Discussion started: 29 June 2026

proportion of this module was significantly reduced. Consequently, the advection module has emerged as a computational hotspot with comparable time consumption to the optimized chemistry module. To address this shift, this study focuses on enhancing the advection module performance in EPICC-Model V1.6.0 via GPU-HADVPPM4HIP V1.0 coupling and GPU-optimized strategies. Sect. 2 details the EPICC-Model's computational framework, baseline performance tests, and the heterogeneous computing platform employed in this research. Sect. 3 elaborates on the optimization framework specifically designed for the computational characteristics of the EPICC-Model advection module. Sect. 4 presents experimental results, including simulation performance and computational performance analysis.

2. The EPICC-Model and experiments

2.1. The framework of the EPICC-Model

The emission and atmospheric processes integrated and coupled community model version V1.6.0 (EPICC-Model V1.6.0; EPICC-Model Working Group, 2025; Wang et al., 2025) is an air quality modeling system specifically designed for air pollution complex in China (Zhu et al., 2023), and developed by the Institute of Atmospheric Physics, Chinese Academy of Sciences based on the Earth System Numerical Simulation Facility (EarthLab, Chai et al., 2021). The model framework is fundamentally based on the species continuity equation and is used to simulate the complex physical and chemical processes of pollutants in the atmosphere. These processes include emissions, advection, diffusion, aerosol processes, gas-phase chemistry, and deposition. The EPICC-Model V1.6.0 adopts a modular architecture developed using Fortran programming language, a high-performance computing language specifically designed for scientific applications. The model code is open-source and shared (EPICC-Model Working Group,2026). This open-source code repository enables rapid integration of novel mechanisms and modules proposed by diverse research groups, thereby enhancing collaborative development efficiency.

The computational framework and workflow of the EPICC-Model V1.6.0 are illustrated in Figure 1. The system primarily comprises three components: model inputs, physical-chemical processes, and outputs analysis. Model input data include emissions, meteorological data, and other datasets. Emissions inventories such as the Multi-resolution Emission Inventory for China (MEIC,

https://doi.org/10.5194/egusphere-2026-3368
Preprint. Discussion started: 29 June 2026

Li et al., 2017), the Emissions Database for Global Atmospheric Research (EDGAR, Crippa et al., 2024), the HTAP (Crippa et al., 2023), and the Inversed Emission Inventory for Chinese Air Quality (CAQIEI, Kong et al., 2024) can be utilized. Meteorological data are predominantly derived from simulations generated by the mesoscale Weather Research and Forecasting (WRF) model. Other datasets encompass configuration files, terrain data, TUV photolysis data, as well as initial conditions (IC) and boundary conditions (BC). Physical-chemical processes primarily include horizontal advection, vertical diffusion, dry deposition, wet scavenging, gas-phase chemistry, aqueous-phase chemistry, heterogeneous reactions, inorganic aerosol thermodynamics, etc. For the vertical diffusion module, either the scheme of Byun and Dennis (1995) or the YSU scheme (Hong et al., 2006) can be selected to calculate the turbulent vertical diffusion coefficient. The dry deposition module can employ either the scheme of Wesely (1989) or Zhang et al. (2003) to compute deposition velocities. The gas-phase chemistry module offers the option to utilize either the CBM-Z (Zaveri and Peters, 1999) or CB6r5 (Yarwood et al., 2020) chemical mechanisms. For heterogeneous reactions, the model defaults to the scheme of Li et al. (2012). Additionally, it integrates mechanisms for HONO heterogeneous chemical reactions (Zhang et al., 2022), sulfate heterogeneous chemical reactions (Li et al., 2018), and N_2O_5 heterogeneous hydrolysis (Yang et al., 2024). Inorganic aerosol is simulated using the ISORROPIA aerosol thermodynamic model (Nenes et al., 1998). The aqueous-phase chemistry module originates from the Regional Acid Deposition Model (RADM, Chang et al., 1987). Regarding model output analysis, the EPICC-Model can generate pollutant concentration fields, pollutant deposition fluxes, process analysis data, and source apportionment data. For a comprehensive technical description of the model architecture and implementation details, refer to the EPICC-Model Working Group (2025).

https://doi.org/10.5194/egusphere-2026-3368
Preprint. Discussion started: 29 June 2026

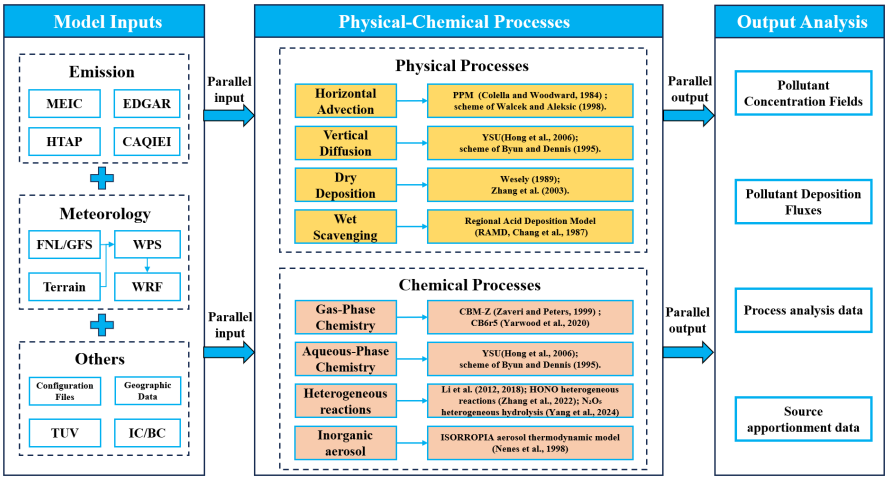

Figure 1. The computational framework and workflow of the EPICC-Model V1.6.0. In the section of physical-chemical processes, yellow represents the physical module, and orange indicates the chemical module.

For the horizontal advection module that is the focus in this study, two high-precision numerical schemes are available, the positive-definite mass-conservative differencing scheme (Walcek and Aleksic, 1998) and the piecewise parabolic method (PPM, Colella and Woodward, 1984). The PPM scheme, an extension of high-order Godunov's method, operates by partitioning the integration domain into subregions and approximating solutions using parabolic functions. Renowned for its numerical precision and robustness in complex fluid dynamics, this classic algorithm has been widely adopted in atmospheric chemistry models including the latest CMAQ and CAMx (Appel, et al., 2021; Emery, et al., 2024). Within the EPICC-Model V1.6.0 framework, the advection module sequentially executes transport processes in the *x*-direction and *y*-direction. It employs species-specific PPM solvers (HADVPPM subroutine) for gaseous species, inorganic aerosols, organic aerosols, dust, and sea salt. Our previous studies have demonstrated a significant acceleration performance of PPM solver in the CAMx model through HIP heterogeneous programming technologies for GPU-like (Cao et al., 2024).

2.2. Benchmark performance of testing

As mentioned above, Cao et al. (2025) implemented the fourth-order Rosenbrock solver for the gas-phase chemistry module in the EPICC-Model, employing the CBM-Z chemical mechanism.

https://doi.org/10.5194/egusphere-2026-3368
Preprint. Discussion started: 29 June 2026

Through code restructure from Fortran to standard C programming language and implementation of the HIP heterogeneous programming framework, the computational efficiency of the gas-phase chemistry module improved by 2.88 times when accounting for data transfer between CPUs and the GPU-like accelerators.

Figure 2. illustrates the changes in the computational time proportion among modules before and after the heterogeneous parallel implementation of the gas-phase chemistry module on GPU-like accelerators, as reported by Cao et al. (2025). Specifically, Figure 2(a) shows the time proportion of each module in the original Fortran version, while Figure 2(b) presents the corresponding proportion after the gas-phase chemistry module was ported for parallel computing on GPU-like. As shown in Figure 2, the implementation of parallel computing for gas-phase chemistry modules on GPU-like achieved significant efficiency improvements, reducing its computational time proportion from 45.7% to 29.9%. Notably, the computational time proportion of MPI_Barrier synchronization function has decreased from 23.9% to 13.4%. A critical observation emerged regarding the advection module, whose computational time proportion increased from 13.3% to 25.0%, establishing it as a new performance bottleneck comparable to the optimized chemistry module. This performance shift necessitates subsequent optimization efforts focusing on heterogeneous porting and parallel acceleration of the PPM scheme for GPU-like architectures within the EPICC-Model framework, aiming to enhance the computational efficiency of the advection module.

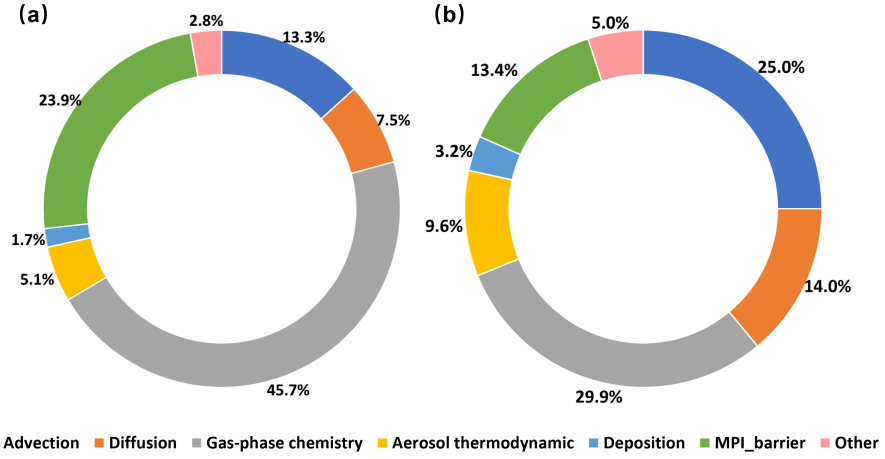

Figure 2. The computational time proportion among modules (a) for the Fortran version and (b)

https://doi.org/10.5194/egusphere-2026-3368
Preprint. Discussion started: 29 June 2026

after implementing the gas-phase chemistry module on GPU-like accelerators for parallel computation.

2.3. Hardware platform and software environment of experiments

All performance testing of the EPICC-Model V1.6.0 and heterogeneous adaptation and optimization studies of the advection module on GPU-like accelerators were conducted at the Earth System Numerical Simulation Facility (EarthLab, Chai et al., 2021). Jointly developed by the Institute of Atmospheric Physics, Chinese Academy of Sciences and collaborating institutions, this platform, specifically designed for earth system modeling and high-resolution regional environmental simulation, employs a CPU and GPU heterogeneous architecture. Detailed hardware components and software environment are presented in Table 1. The Chinese domestic CPUs and GPU-like accelerators used in this studying are the first-generation versions. Each GPU-like node contains two China's domestic CPU processors and two GPU-like accelerators (Cao et al., 2024) interconnected via PCIe 4.0 buses. The software stack employs Intel OneAPI 2021.3.0 toolkit for CPU code compilation and dtk-23.04.1 toolkit for GPU-like code compilation, ensuring full compatibility with heterogeneous computing paradigms.

Table 1 The hardware components and software environment for the dedicated accelerator node on the EarthLab.

	CPU	**GPU**
Hardware components	two of China's domestic CPU processors，2.0 GHz, 32 cores	two of GPU-like accelerators，3840 computing units，16 GB memory
Software environment	Intel OneAPI 2021.3.0 toolkit	dtk-23.04.1

Compared to CPU processors, GPU-like accelerators demonstrate superior capability in launching massive thread-level parallelism. Similar to the NVIDIA GPU architectures (NVIDIA, 2020), these GPU-like accelerators employ a three-level parallelism hierarchy comprising grids, blocks, and threads, which collaboratively execute parallel computations through coordinated indexing. Specifically, a computational grid is partitioned into multiple thread blocks with three-dimensional coordinates, each thread block containing an array of three-dimensional indexed threads. As the fundamental execution unit, individual threads perform concrete computational tasks, each possessing a unique index ID that precisely determines its spatial position within the thread

https://doi.org/10.5194/egusphere-2026-3368
Preprint. Discussion started: 29 June 2026

block hierarchy. Consequently, the design of hierarchical indexing schemes coordinating blocks and threads constitutes a critical challenge in achieving efficient parallel computation for three-dimensional numerical modeling grids.

Analogous to the AMD's ROCm software stack (AMD, 2023), the dtk-23.04.1 toolkit (Cao et al., 2024) includes programming models, tools, compilers, libraries, and runtimes for artificial intelligence and high-performance computing applications on GPU-like accelerators. Mirroring ROCm's design paradigm, dtk-23.04.1 adopts the HIP programming language as its application programming interface (API). This implementation leverages the Single-Instruction Multiple-Thread (SIMT) execution model to effectively manage and coordinate massive thread parallelism on GPU-like accelerators.

3. Implementation details

3.1. Description of the heterogeneous porting and optimization scheme

The heterogeneous porting and parallel optimization schemes of this study are illustrated in Figure 3. Similar to the heterogeneous porting approach for the advection module of the air quality model CAMx on GPU-like accelerators (Cao et al. 2024), the first step involved the porting and adaptation of the HADVPPM advection solver from the EPICC-Model V1.6.0 to GPU-like accelerators. Firstly, the Fortran code of the HADVPPM subroutine was reconstructed using standard C programming language, followed by implementing parallel computing on GPU-like accelerators through the HIP API. Similar to CUDA program execution on NVIDIA GPUs, the implementation of GPU-HADVPPM4HIP V1.0 on GPU-like accelerators follows four key steps: (1) Device memory allocation via the hipMalloc interface, (2) Data transfer from CPU to GPU-like accelerator through hipMemcpy operations, (3) Parallel computation using kernel launching (hipLaunchKernelGGL) with thread-index-based parallel processing after successful data transmission, and (4) Final data retrieval from GPU back to CPU through hipMemcpy operations.

Following the implementation of GPU-HADVPPM4HIP V1.0 parallel computing on GPU-like accelerators, the second phase involves architecture-specific parallel optimizations tailored for GPU-like characteristics. Three optimization strategies were sequentially implemented to fully exploit the SIMT vectorization parallelism of GPU-like accelerators, thereby enhancing the

https://doi.org/10.5194/egusphere-2026-3368
Preprint. Discussion started: 29 June 2026

computational performance of the EPICC-Model advection module. These strategies include: (1) reducing the frequency of communication between the CPU and GPU, (2) collaborative indexing between threads and blocks, and (3) hybrid parallelization of "MPI+HIP". For systematic reference, three progressively optimized configurations were designated, namely HIP-Ori, HIP-Opt1, and HIP-Opt2. The HIP-Ori is baseline implementation after GPU-HADVPPM4HIP V1.0 integration into EPICC-Model without optimizations. The HIP-Opt1 is the version implementing reduced CPU-GPU communication frequency. The HIP-Opt2 is the enhanced version incorporating collaborative thread-block indexing. The hybrid "MPI+HIP" parallelization strategy was implemented across all three heterogeneous versions to enhance parallel scalability of the EPICC-Model V1.6.0 on the EarthLab.

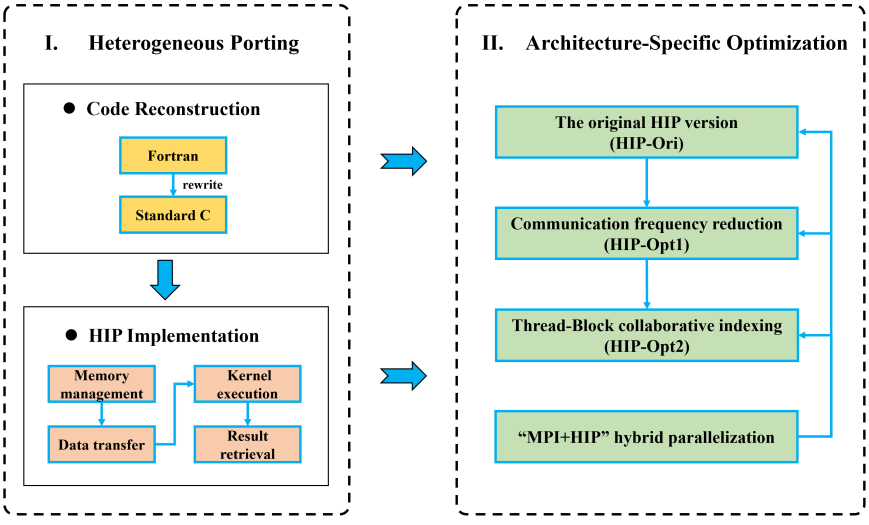

Figure 3. Heterogeneous porting and parallel optimization scheme of advection module in the EPICC-Model V1.6.0.

3.2. HIP-Opt1: Communication frequency reduction

Influenced by the evolutionary trajectory of high-performance computing, most geoscientific numerical models, including the EPICC-Model, are predominantly coded in Fortran and designed for general-purpose CPU architectures. These models typically execute computations through grid-wise loop iterations. Taking the HADVPPM subroutine in the EPICC-Model as an example, its

https://doi.org/10.5194/egusphere-2026-3368
Preprint. Discussion started: 29 June 2026

computational kernel is structured with triple nested loops progressing from innermost to outermost: species loop (loop_species), latitudinal grid loop (loop_j), and vertical grid loop (loop_k). The EPICC-Model innovatively categorizes atmospheric pollutants within the species loop into five distinct classes: gaseous species (74 chemical constituents), inorganic aerosols (14 species subdivided into coarse- and fine-mode particle sizes), organic aerosols, dust aerosols (8 species across 4 size bins), and sea salt aerosols (11 species across 4 size bins).

The EPICC-Model calculates the advection process through looping of chemical-specified variables, which has relatively low computational efficiency. A benchmark test using a two nested grid configuration (horizontal grids: d01=228×165, d02=465×300) indicated that each timestep requires approximately 9.8 million calls of the HADVPPM subroutine for advection processes in both *x*-direction and *y*-direction. Consequently, the HIP-Ori version, generated by integrating GPU-HADVPPM4HIP V1.0 into the EPICC-Model, incurs 9.8 million CPU-GPU data transfers per timestep. Benchmark tests demonstrated that the computational time for 1-hour integration increased from 1,015.0 seconds in the original Fortran version to 20,400.3 seconds under HIP-Ori version, with frequent CPU-GPU communication identified as a primary performance bottleneck. To address this critical bottleneck, our optimization framework prioritizes architectural redesign of the advection module's loop hierarchy, strategically reducing communication frequency while increasing data transfer sizes to better exploit GPU computational capacity.

Figure 4 illustrates the code-level implementation of CPU-GPU communication optimization, with panel (a) depicting the HIP-Ori baseline and panel (b) presenting the optimized HIP-Opt1 version. In the two nested-domain case, the HIP-Ori configuration required approximately 4.9 million GPU calls for *x*-direction advection alone. To mitigate this computational overhead, we restructured the advection module's loop architecture and expanded array dimensionality. The HIP-Opt1 optimization framework implements multidimensional array restructuring, beginning with the dimensional expansion of concentration variables from their original 1D representations (Q01d) in HIP-Ori to 4D/5D configurations (Q04d/Q05d), while auxiliary parameters such as grid area adjustment vector (area) and interfacial area adjustment vector (areav) are similarly upgraded from 1D to 3D structures. Prior to GPU execution, these variables undergo systematic multidimensional reorganization, as demonstrated by the transformation of gaseous concentration variables from

https://doi.org/10.5194/egusphere-2026-3368
Preprint. Discussion started: 29 June 2026

Q01d_gas(*i*) to Q04d_gas (*i, j, k, species*) in Figures 4(a)-(b). This architectural redesign enables complete *x*-direction advection computation through a single GPU call per pollutant category. Consequently, the total GPU calls for both *x* and *y* direction advection decrease from approximately 9.8 million in HIP-Ori to 10 in HIP-Opt1, achieved through one GPU call per spatial dimension across five pollutant categories, thereby optimizing computational efficiency through batched multidimensional data processing.

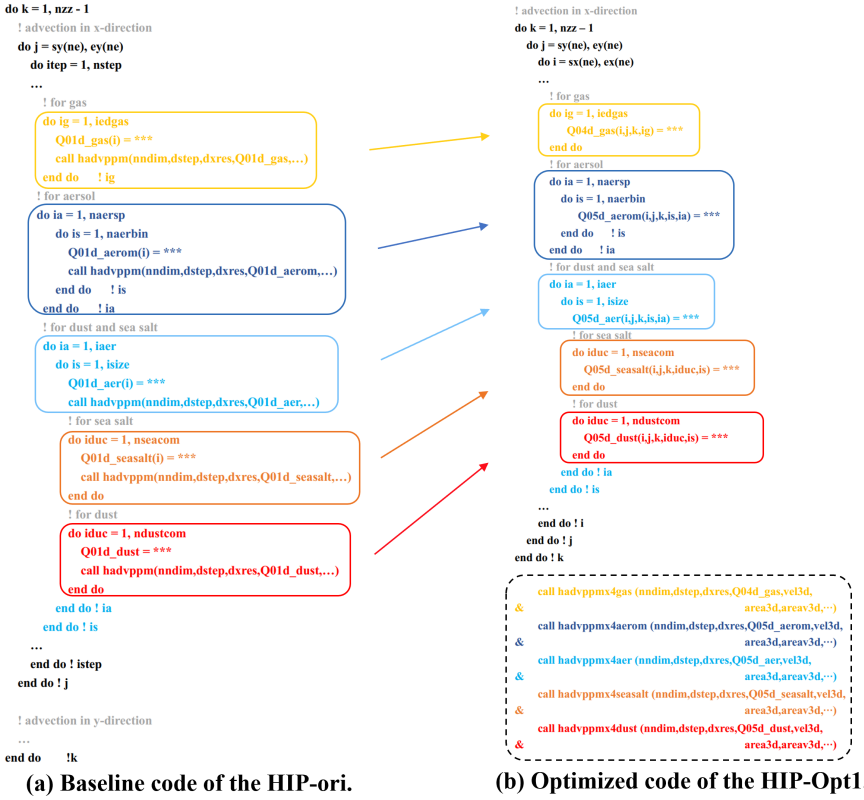

(a) Baseline code of the HIP-ori. **(b) Optimized code of the HIP-Opt1.**

Figure 4. The code-level implementation of CPU-GPU communication optimization. Panel (a) is the baseline Fortran code of the HIP-ori Panel (b) is the optimized Fortran code of the HIP-Opt1.

3.3. HIP-Opt2: Thread and block coordinated indexing

The architectural advantage of GPU-like accelerators manifests in their capacity to support massive thread concurrency for parallel computing. To leverage this capability, the coordinated thread-block indexing methodology which proposed by Cao et al. (2023) was implemented, whereby in which each grid cell in the two-dimensional horizontal plane is assigned a dedicated

https://doi.org/10.5194/egusphere-2026-3368
Preprint. Discussion started: 29 June 2026

thread. Specifically, blocks were configured based on the meridional grid dimension, with each block allocated threads corresponding to the zonal grid count. This hierarchical parallelization strategy achieves comprehensive full parallel processing of across the two-dimensional planar grid structure through coordinated thread-block resource allocation. Furthermore, given that GPUs are well-suited for large-scale matrix parallel computations without data dependencies, prior to implementing parallel computation on a two-dimensional grid using thread and block coordinated indexing, we decoupled the iterative computations present in the advection module by introducing intermediate variables. This ensures computational independence at each step, meaning that the computation of the next step does not depend on the results of the previous step, thereby fully leveraging the multi-thread parallel computing capability of the GPU.

3.4. “MPI+HIP” hybrid parallelization

The recent advancements in GPU technology have solidified the dominance of "CPU+GPU" heterogeneous architectures in global high-performance computing, with 9 out of the top 10 supercomputers in 2024 utilizing heterogeneous configurations (Top 100, 2024). These large-scale heterogeneous clusters typically deploy one or multiple GPU accelerators per compute node. Aligned with this trend, EarthLab employs heterogeneous architecture in its dedicated computing nodes, integrating China’s domestic CPUs with GPU-like accelerators. To maximize GPU utilization and enhance the parallel scalability of the EPICC-Model on heterogeneous clusters, an “MPI+HIP” hybrid parallelization scheme was designed tailored for EarthLab, inspired by the “MPI+CUDA” approach proposed by Cao et al. (2023) for the CAMx model.

In the original Fortran version of EPICC-Model, the entire simulation domain is decomposed into subdomains using MPI, with each CPU process responsible for computations, including those of the advection module, within one subdomain. In this study, after MPI domain decomposition, we offloaded the advection module computations originally performed on the CPU to China’s domestic GPUs through heterogeneous porting, thereby enabling parallel execution of the advection module on GPUs. Considering future high-resolution applications with large-scale data, assigning a single GPU to multiple CPU processes could lead to data-transfer contention and potential GPU memory overflow. Therefore, we adopted an “MPI+HIP” hybrid parallelization approach, in which each participating CPU process is assigned a dedicated GPU accelerator. This design expands the parallel

https://doi.org/10.5194/egusphere-2026-3368
Preprint. Discussion started: 29 June 2026

computing capacity of the model on heterogeneous clusters and makes full use of GPU resources. The implementation can be summarized in three main steps: (1) Obtain the MPI process rank information, as well as the number and indices of GPUs available on each compute node; (2) Based on the MPI process rank and using the remainder function in standard C, determine the number and indices of GPUs to be launched; (3) Map each MPI process to a specific GPU index, thereby realizing the "one CPU process – one GPU" configuration in the MPI+HIP hybrid parallel scheme.

As illustrated in Figure 5, taking the d02 domain configured in Section 4.1 with 8 CPU processes and 8 GPU-like accelerators as an example: the EPICC model decomposes the simulation domain into 8 subdomains using the MPI software standard, with each CPU process handling its assigned subdomain. During the execution of the advection module, the "MPI+HIP" hybrid parallel scheme allocates one GPU accelerator to each CPU process. Computational tasks originally performed by the CPU are offloaded to the corresponding GPU; after the advection computations are completed, the results are returned to the CPU.

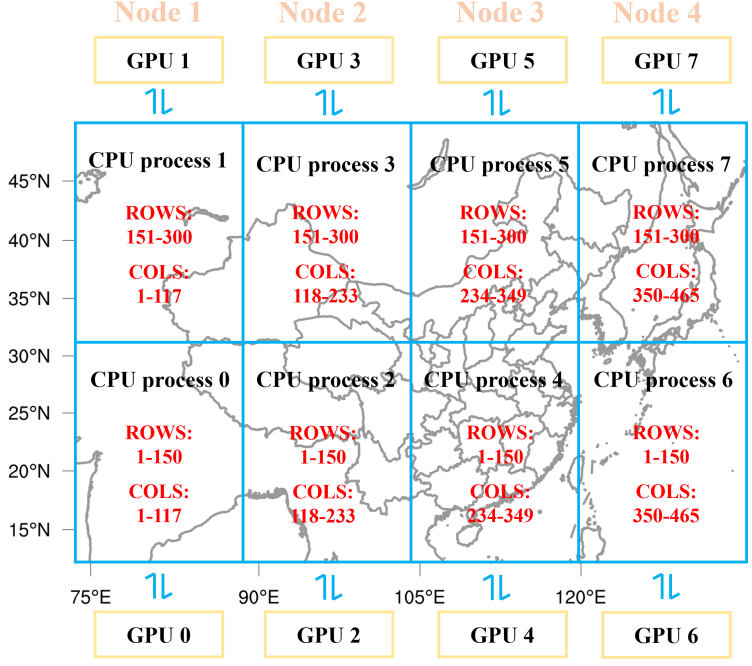

Figure 5. An example schematic of domain subdivision and mapping to CPU processes, where each CPU process is equipped with a GPU-like accelerator.

https://doi.org/10.5194/egusphere-2026-3368
Preprint. Discussion started: 29 June 2026

4. Experimental results

4.1. Experimental setup

The centre of the simulation domain is located at (35 °N, 105 °E) and its two true latitude lines are 25 °N and 45 °N, respectively. The EPICC-Model V1.6.0 employs a two-nested configuration, the first domain (d01) covers East Asia with a 45 *km* × 45 *km* horizontal resolution on 228×165 grid cells. The lower left corner of the second domain has its starting positions in the grid of the first domain as 36 and 39, respectively, and the second domain focuses on China with a 15 *km* × 15 *km* horizontal resolution on 465×300 grid cells. In vertical, 20 terrain-following layers are configured with the height of the top layer set to 20 *km* and six layers below 1 *km*. The numerical simulation was conducted from 00:00 UTC July 1 to 23:00 UTC on 31 July, 2021, spanning a total duration of 744 hours. The initial 168-hour period was allocated for model spin-up. The MEIC emission inventory (Li et al., 2017) was adopted as the emission input, and baseline year is 2019. The numerical schemes selected during the EPICC-Model V1.6.0 simulations are listed in Table 2. Furthermore, the $PM_{2.5}$ and O_3 observations are from the China National Environmental Monitoring Centre, which provides hourly $PM_{2.5}$ and O_3 observations for eight cities in China. The station information, including station name and its latitude and longitude, is listed in Table 3. Meteorological inputs are generated using the Weather Research and Forecasting (WRF, Skamarock et al., 2008) model, a mesoscale numerical weather prediction system, and is widely adopted in both theoretical research and operational forecasting. This study employed the WRF version 3.9.1, and the model domain configurations maintains identical nesting architecture and spatial coverage as the EPICC-Model.

Table 2. The physical and chemical numerical schemes selected during EPICC-Model V1.6.0 simulation.

Process	Numerical schemes
Horizontal advection	PPM (Colella and Woodward, 1984)
Vertical diffusion	YSU scheme (Hong et al., 2006)
Gas-phase chemistry	CBM-Z (Zaveri and Peters, 1999)
Aqueous-phase chemistry and wet deposition	RADM (Chang et al., 1987)
Dry deposition	Scheme of Wesely (1989)
Inorganic aerosol thermodynamic partitioning	ISORROPIA v1.7 (Nenes et al., 1998)

https://doi.org/10.5194/egusphere-2026-3368
Preprint. Discussion started: 29 June 2026

Table 3. The names and latitude-longitude information of the $PM_{2.5}$ and O_3 observation stations.

Name	Latitude (°N)	Longitude (°E)
Beijing	40.2865	116.1700
Taiyuan	37.7394	112.5583
Hangzhou	30.3058	120.3480
Hefei	31.7386	117.2780
Fuzhou	25.9664	119.5189
Qingdao	36.1032	120.3664
Guangzhou	23.5538	113.5890
Kunming	24.9786	102.7997

4.2. Simulation performance analysis

4.2.1. Error analysis of the GPU-HADVPPM4HIP

As elaborated in Sect. 3.1, the implementation of the HADVPPM Fortran code on GPU-like comprises two principal phases. Initially, the Fortran code undergoes reconstruction using standard C programming language through a Fortran-to-C conversion process. Subsequently, the standard C-version HADVPPM program is adapted to GPU-like accelerators through C-to-HIP expansion employing the HIP heterogeneous programming technology. Following successful GPU adaptation, the offline precision verification was conducted to compare computational accuracy among three implementations, the original Fortran source code, restructured standard C code, and HIP-accelerated code. To ensure input consistency, a dedicated Fortran program was developed to generate identical input datasets, including 100 double-precision floating-point numbers, for all three implementations. Each implementation executed a complete advection integration computation, with subsequent output recording and analysis. Therefore, the absolute errors (AE) and relative errors (RE) presented in Table 4 represent the average values computed from the 100 double-precision floating-point results produced by the original Fortran code, restructured standard C code, and HIP-accelerated code of the HADVPPM program after performing the advection solution computation under the given input conditions.

Notably, both Fortran and C implementations were executed on China's domestic CPUs and compiled using the Intel OneAPI 2021.3.0 tookit, while GPU-HADVPPM4HIP was compiled with

https://doi.org/10.5194/egusphere-2026-3368
Preprint. Discussion started: 29 June 2026

the dtk-23.04.1 toolkit for GPU execution. For enhanced analytical rigor, we further implemented compilation with -O0 and -O3 optimization flags. The -O0 flag maintains default compilation settings without code optimization, whereas -O3 flag enables more aggressive loop and memory-access optimizations, such as scalar replacement, loop unrolling (Intel Software, 2018).

Table 4 presents the mean absolute error (AE) and relative errors (RE) in computational precision between the Fortran and standard C implementations (F-to-C), standard C and HIP implementations (C-to-HIP), and Fortran and HIP implementations (F-to-HIP) of the HADVPPM program under two compilation configurations. Notably, the -O3 optimization flag prioritizes computational performance through code optimization at the expense of precision degradation. Consequently, the AE and RE values for all three porting processes (F-to-C, C-to-HIP, and F-to-HIP) under the -O0 configuration flag are systematically lower than those under -O3 flag. For instance, between the Fortran and HIP implementations, the AE and RE under -O0 flag are measured at 1.4×10^{-7} and 4.3×10^{-7}%, respectively. However, when compiled with -O3 flag, these errors increase significantly to 3.1×10^{-7} and 2.5×10^{-6}%, respectively. Similar error escalation patterns are observed in the F-to-C and C-to-HIP comparisons under -O3 optimization flag. This phenomenon aligns with expectations, as aggressive compiler optimizations (e.g., loop unrolling and memory access reorganization) may introduce numerical instability through altered operation sequences and reduced intermediate precision preservation.

Furthermore, it is noteworthy that across both -O0 and -O3 compilation configurations, the AE and RE values of the F-to-C process consistently exceed those of the C-to-HIP process. This indicates that the computational errors introduced during the heterogeneous porting of the HADVPPM Fortran code from domestic CPUs to GPU-like accelerators predominantly originate from the Fortran-to-C transcoding phase. For instance, under the -O0 configuration, the AE and RE for F-to-C are measured at 1.5×10^{-7} and 5.1×10^{-7}%, respectively, whereas those for C-to-HIP are significantly smaller, at -9.5×10^{-9} and -8.0×10^{-8}%, respectively. This discrepancy arises from inherent differences between Fortran and C in programming paradigms and data precision management. The Fortran-to-C code restructuring involves two fundamentally distinct programming languages, differing in object-oriented design philosophies and numerical representation conventions, thereby introducing computational inaccuracies. In contrast, the HIP

https://doi.org/10.5194/egusphere-2026-3368
Preprint. Discussion started: 29 June 2026

programming model, analogous to NVIDIA CUDA, is inherently an extension of standard C. As detailed in Sect. 3.1, HIP achieves GPU compatibility by augmenting standard C programming language with critical GPU-specific functionalities, such as memory allocation and data transfer operations. Since HIP code essentially constitutes an enhanced standard C framework, the C-to-HIP adaptation introduces minimal computational bias, resulting in markedly lower error compared to the F-to-C transformation.

Table 4. Comparative of mean AE and RE across compilation configurations for F-to-C, C-to-HIP, and F-to-HIP Processes.

	AE			RE (%)		
	F-to-C	C-to-HIP	F-to-HIP	F-to-C	C-to-HIP	F-to-HIP
-O0	1.5×10^{-7}	-9.5×10^{-9}	1.4×10^{-7}	5.1×10^{-7}	-8.0×10^{-8}	4.3×10^{-7}
-O3	5.4×10^{-7}	-2.4×10^{-7}	3.1×10^{-7}	2.8×10^{-6}	-2.9×10^{-7}	2.5×10^{-6}

By coupling GPU-HADVPPM4HIP V1.0 into the EPICC-Model and implementing optimizations—such as reducing the communication frequency between CPUs and domestic GPUs, adopting thread and block coordinated indexing, and employing "MPI+HIP" hybrid parallelization—we developed the HIP-Opt2 version. Using identical input data and model configurations, the differences in simulation results between the HIP-Opt2 version and the original Fortran version were compared in a real-world case study. The model input data and configurations were set as described in Section 4.1, with the simulation period covering 24 hours from 00:00 to 23:00 UTC on July 1, 2021.

Figures 6 and 7 present the simulated concentrations of gases (e.g., HONO, SO_2, NO_2, NH_3) and aerosols (e.g., BC, $PM_{2.5}$, ASO_4, ANH_4) after a 24-hour integration by both the HIP-Opt2 and the original Fortran versions, along with the Absolute Errors (AEs) between the two model versions. As visually evident from the figures, the results from HIP-Opt2 after the 24-hour integration are in close agreement with those from the original Fortran version. For the vast majority of grid points, the AEs for gases and aerosols remain within ±0.1 ppbV or ±0.1 $\mu g \cdot m^{-3}$.

To further evaluate the suitability of HIP-Opt2 for scientific research, we followed the methodologies of Wang et al. (2021) and Cao et al. (2024) by introducing two metrics: the root mean square error (RMSE) and the standard deviation (std). The ratio of RMSE to std was calculated to quantify the scientific applicability of HIP-Opt2. Here, RMSE represents the error between HIP-

https://doi.org/10.5194/egusphere-2026-3368
Preprint. Discussion started: 29 June 2026

Opt2 and the original Fortran version for different species, while std denotes the standard deviation of each species in the Fortran version. Taking NO_2 as an example, a very small RMSE/std ratio indicates that the computational deviation introduced by heterogeneous parallel acceleration is negligible compared to the inherent spatial variability of NO_2. This implies that such minor computational errors do not compromise the model's utility in scientific research. Table 5 lists the RMSE, std, and their ratios for the aforementioned gases and aerosols. The RMSE/std ratios for these species range from 10^{-5}% to 10^{-2}%. Specifically, BC exhibits the smallest ratio at 4.8×10^{-5}%, while ASO_4 shows the largest ratio, yet only at 7.0×10^{-2}%. The RMSE/std ratios for all species in HIP-Opt2 are comparable to those reported by Cao et al. (2024), demonstrating that the simulation results from the HIP-Opt2 version are fully suitable for scientific applications.

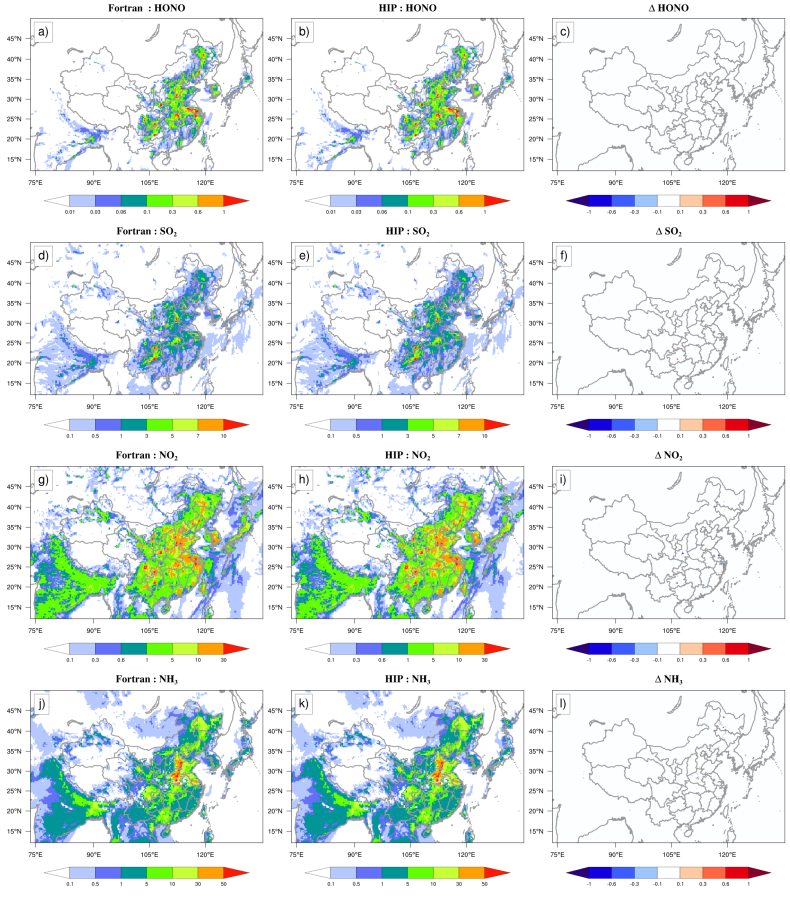

Figure 6. HONO, SO_2, NO_2, and NH_3 concentrations outputted by the EPICC-Model for the Fortran

https://doi.org/10.5194/egusphere-2026-3368
Preprint. Discussion started: 29 June 2026

and HIP-Opt2. versions. Panels (a), (d), (g), and (j) are from the Fortran version. Panels(b), (e), (h), and (k) are from the HIP-Opt2. version. Panels (c), (f), (i), and (l) are the absolute errors (AEs) between the Fortran and HIP-Opt2. Versions.

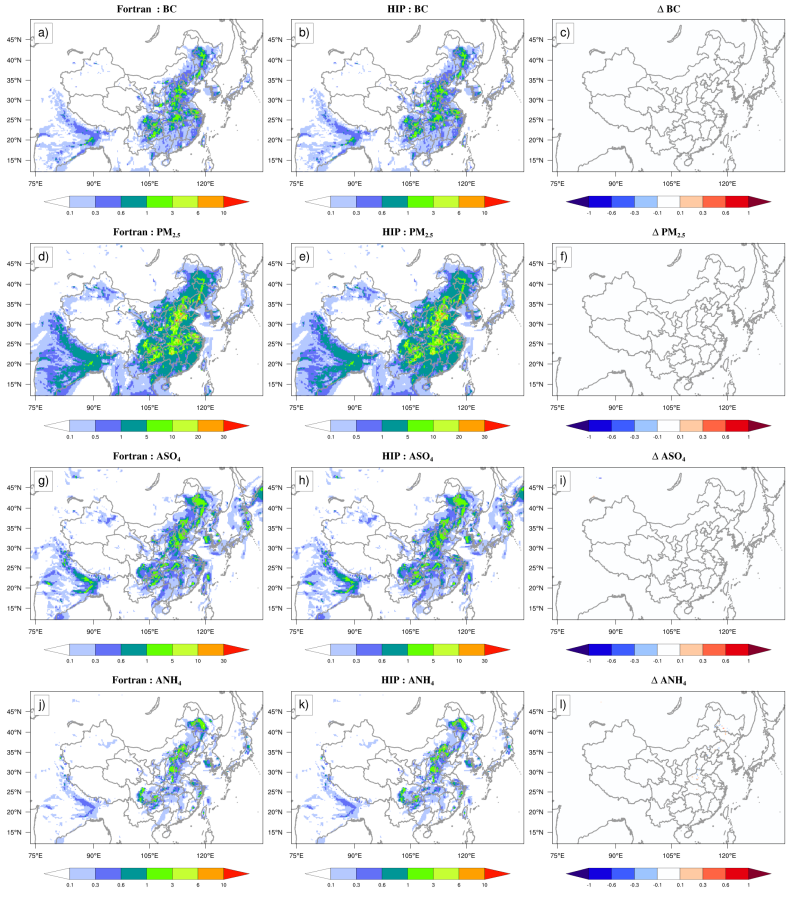

Figure 7. BC, $PM_{2.5}$, ASO_4, and ANH_4 concentrations outputted by the EPICC-Model for the Fortran and HIP-Opt2. versions. Panels (a), (d), (g), and (j) are from the Fortran version. Panels(b), (e), (h), and (k) are from the HIP-Opt2. version. Panels (c), (f), (i), and (l) are the absolute errors (AEs) between the Fortran and HIP-Opt2 versions.

Table 5. The root mean square error (RMSE) between the Fortran and HIP-Opt2. versions, standard deviation (std) of the Fortran version, and the RMSE and std ratio.

	RMSE	std	RMSE/std (%)

https://doi.org/10.5194/egusphere-2026-3368
Preprint. Discussion started: 29 June 2026

HONO (ppbV)	2.1×10^{-5}	0.1	2.1×10^{-2}
SO_2 (ppbV)	3.3×10^{-5}	0.7	4.5×10^{-3}
NO_2 (ppbV)	2.8×10^{-4}	3.4	8.3×10^{-3}
NH_3 (ppbV)	9.6×10^{-5}	4.1	2.4×10^{-3}
BC ($\mu g \cdot m^{-3}$)	9.7×10^{-8}	0.2	4.8×10^{-5}
$PM_{2.5}$ ($\mu g \cdot m^{-3}$)	4.4×10^{-6}	1.9	2.3×10^{-4}
ASO_4 ($\mu g \cdot m^{-3}$)	1.7×10^{-4}	0.2	7.0×10^{-2}
ANH_4 ($\mu g \cdot m^{-3}$)	1.1×10^{-4}	0.2	5.8×10^{-2}

4.2.2. Simulation performance verification of the EPICC-Model

After parallelizing the HADVPPM program in the air quality model CAMx on GPU-like accelerators, Cao et al. (2024) conducted comparative analyses of simulation results between NVIDIA GPUs and domestic GPUs through offline and coupled testing approaches. Although both experimental results indicated smaller computational errors introduced by China's domestic GPUs, the study did not validate the discrepancies between CAMx simulation results and actual observational data, particularly regarding model performance in real-case scenarios. To address this gap, the current study integrates GPU-HADVPPM4HIP V1.0 into the EPICC-Model V1.6.0 and performs one-month real-case simulations following the experimental configuration described in Sect. 4.1. This serves dual purposes: firstly, to verify the computational stability of EPICC-Model V1.6.0 in cross-architecture heterogeneous cluster environments using China's domestic hardware, and secondly, to evaluate the model's pollutant simulation performance through observational validation. For observational data, we collected $PM_{2.5}$ and O_3 observations from major Chinese cities including Beijing, Taiyuan, Hangzhou, Hefei, Fuzhou, Qingdao, Guangzhou, and Kunming, implementing quality control procedures following the methodology established by Wu et al. (2018). Regarding simulation data, we extracted model outputs from grid cells in the d02 domain corresponding to the geographical coordinates of monitoring stations.

Figure 8 and Figure 9 along with Table 6, present the time series comparisons between daily simulated and observed $PM_{2.5}$ and O_3 concentrations, as well as relevant statistical metrics, following the one-month simulation after coupling GPU-HADVPPM4HIP V1.0 to the EPICC-Model V1.6.0. The formulas for calculating statistical parameters are detailed in the Supplementary Materials. For daily $PM_{2.5}$ concentrations, the EPICC-Model V1.6.0 demonstrated robust simulation

https://doi.org/10.5194/egusphere-2026-3368
Preprint. Discussion started: 29 June 2026

performance across most cities, with slight overestimations observed in Beijing and Hefei. Notably, the model effectively captured the temporal variations of $PM_{2.5}$ in Fuzhou, achieving a root mean square error (RMSE) of 3.9 $\mu g \cdot m^{-3}$ and a correlation coefficient (r) of 0.89. Across the eight cities, the mean RMSE and r between simulated and observed $PM_{2.5}$ were 9.4 $\mu g \cdot m^{-3}$ and 0.70, respectively. Regarding daily maximum 8-hour average (MDA8) O_3 concentrations, the model exhibited minor underestimations at certain times in Taiyuan, and Hefei but performed well in Beijing, Fuzhou, Qingdao, and Guangzhou. In Qingdao and Guangzhou, the correlation coefficient between simulated and observed O_3 reached 0.91 and 0.87, with RMSE values of 12.2 ppbV and 8.7 ppbV, respectively. The mean RMSE and r for O_3 across eight cities were 12.1 ppbV and 0.76. These statistical results indicate that the EPICC-Model V1.6.0, integrated with GPU-HADVPPM4HIP V1.0, reasonably reproduces the spatiotemporal characteristics of $PM_{2.5}$ and O_3 concentrations on China's domestic heterogeneous computing clusters.

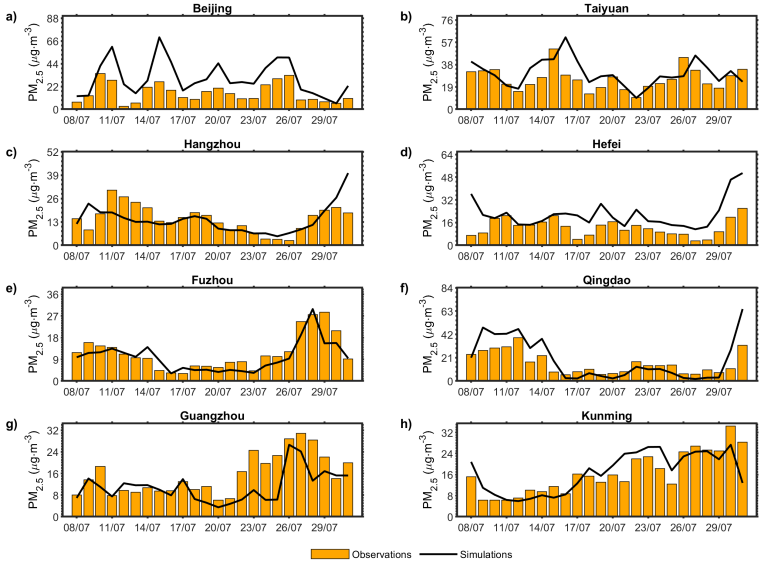

Figure 8. Time series of daily observed and simulated $PM_{2.5}$ concentrations in major cities of China on 8-31 July, 2021. Panels **(a) - (h)** represent Beijing, Taiyuan, Hangzhou, Hefei, Fuzhou, Qingdao, Guangzhou, and Kunming.

https://doi.org/10.5194/egusphere-2026-3368
Preprint. Discussion started: 29 June 2026

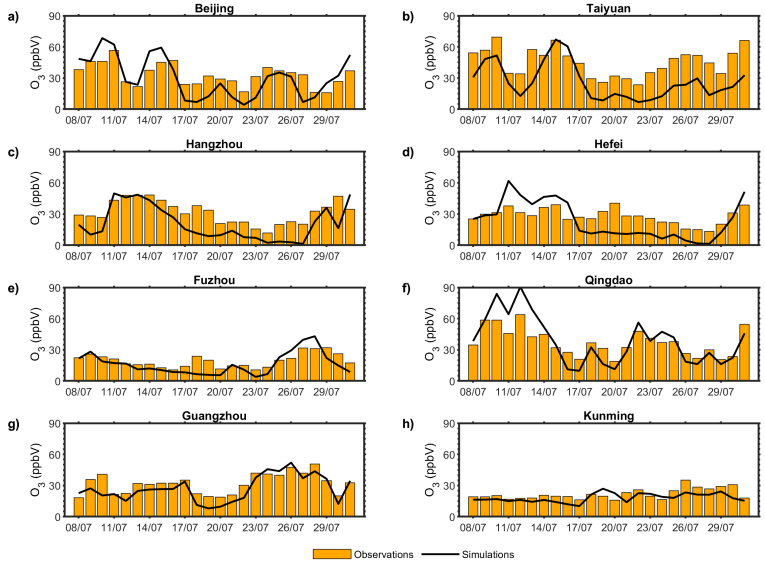

Figure 9. Time series of observed and simulated MAD8 O_3 concentrations in major cities of China on 8-31 July, 2021. Panels **(a) - (h)** represent Beijing, Taiyuan, Hangzhou, Hefei, Fuzhou, Qingdao, Guangzhou, and Kunming.

Table 6. The statistics of the $PM_{2.5}$ and O_3 simulations of EPICC-Model over different eight cities.

	$PM_{2.5}$		**O_3**	
	RMSE ($\mu g \cdot m^{-3}$)	r	RMSE (ppbV)	r
Beijing	17.3	0.84	13.2	0.77
Taiyuan	11.0	0.54	21.6	0.78
Hangzhou	7.4	0.50	14.8	0.80
Hefei	12.4	0.54	14.2	0.70
Fuzhou	3.9	0.87	7.5	0.77
Qingdao	11.0	0.90	12.2	0.91
Guangzhou	7.2	0.65	7.8	0.87
Kunming	5.3	0.76	6.0	0.46
Average	9.4	0.70	12.1	0.76

The underestimations or overestimations of $PM_{2.5}$ and O_3 simulations observed in specific cities and periods are primarily attributable to two factors. First, the coarse model resolution—the horizontal resolution of the d02 domain in this experiment is 15 *km*—hindered the accurate representation of terrain features, meteorological variables, and spatial variations in emission sources. Second, discrepancies exist between the baseline year of the emission inventory and the simulation year. Specifically, the MEIC emission inventory used in this study is based on 2019 data, whereas the simulation year is 2021. For cities with stringent pollution control policies, such as Beijing, the 2019 MEIC inventory may inadequately reflect actual emission reductions achieved by

https://doi.org/10.5194/egusphere-2026-3368
Preprint. Discussion started: 29 June 2026

2021, particularly for pollutants under strict abatement measures. This discrepancy could lead to overestimated simulated concentrations.

4.3. Computational performance analysis

4.3.1. Offline performance comparison

A comparison of offline computational results indicates that the computational errors introduced during the Fortran-to-HIP heterogeneous porting process under both compilation settings are minimal. Specifically, the HADVPPM program exhibits small discrepancies on the order of 10^{-7} when ported from CPU to GPU-like architectures. That is, differences in the computational results only begin to appear at the seventh decimal place. Based on the verified consistency of offline results, the computational performance of the HADVPPM program was further evaluated on domestic CPU and GPU-like under different compilation configurations. To achieve this, Fortran-based test programs were implemented to generate randomized input arrays with varying scales for both Fortran and HIP versions of the HADVPPM program. These random arrays are one-dimensional and contain 10^2, 10^3, 10^4, 10^5, 10^6, 10^7, and 10^8 random numbers. Figure 10 illustrates the computational time and speedup ratios of the HADVPPM program across different compilation options and data scales on domestic CPU and GPU-like. It is explicitly stated that the execution time measurements for the HADVPPM program on the GPU-like exclusively account for the computational time of the kernel functions on the device, while overheads such as GPU memory allocation and host-device data transfer are excluded.

As illustrated in Figure 10(a), under both -O0 and -O3 compilation flags, the SIMT vectorized parallel computing advantages of the GPU-like accelerators become prominent for large data scales exceeding 10^4, demonstrating significantly higher computational efficiency compared to domestic CPU. At a data scale of 10^8 with the -O0 flag, the Fortran-based HADVPPM program required approximately 11.97 seconds to complete computation on the CPU, while the HIP version on the GPU-like achieved the same task in 0.55 seconds, yielding a speedup ratio of 21.87x. The -O3 compilation flag further enhances computational efficiency through automated code optimization, albeit at a slight cost to numerical precision. At the same 10^8 data scale, the Fortran version on the CPU required 2.75 seconds, whereas the HIP version on the GPU completed computations in 0.02 seconds, achieving a remarkable speedup of 128.03×. Notably, the HIP version compiled with -O3

https://doi.org/10.5194/egusphere-2026-3368
Preprint. Discussion started: 29 June 2026

exhibited 556.5x higher efficiency than the Fortran version compiled with -O0 flag. However, for smaller data scales such as 10^2 or 10^3, the architectural advantages of the GPU-like diminish, with computational efficiency comparable to or even lower than that of a CPU. For instance, at a 10^2 scale with the -O3 option, the GPU's performance matched the CPU (speedup ratio is approximately 1). Under the -O0 option, the GPU's speedup dropped to 0.16×, indicating inferior efficiency relative to the CPU. These results underscore that the GPU-like is well-suited for large-scale matrix parallel computing tasks.

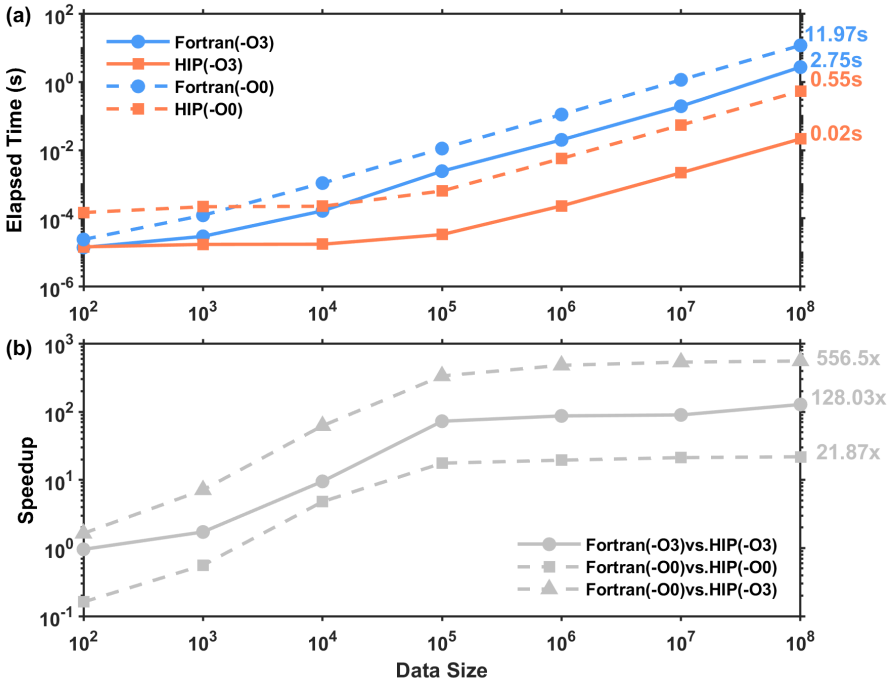

Figure 10. The offline computational time **(a)** and speedup ratios **(b)** of the HADVPPM program across different compilation options and data scales on domestic CPU and GPU-like.

As described in Sect. 3.1, a complete heterogeneous computation of GPU-HADVPPM4HIP V1.0 on the GPU-like involves critical processes such as GPU memory allocation, data transfer between CPU and GPU, and kernel launching for parallel computing. To quantify the overheads of these processes, the time consumption and proportional contributions was analyzed under the -O0 compilation flag and varying data scales. In Figure 11., the label of "Memory Allocation", "Memory Copy", "Kernel", and "Synchronize" represent the processes of memory allocation on the GPU,

https://doi.org/10.5194/egusphere-2026-3368
Preprint. Discussion started: 29 June 2026

bidirectional data transfer between CPU and GPU, kernel launch and parallel computation, as well as thread synchronization within the kernel, respectively.

As shown in Figure 11., for data scales smaller than 10^6, memory allocation dominates the time consumption, exceeding 90% of the total execution time and significantly surpassing the durations of the other three processes. Notably, the time required for memory allocation remains approximately 0.4 seconds regardless of increases in data scale. The dominance of memory allocation at small data scales highlights its fixed overhead nature. This suggests that memory allocation is largely independent of data volume. While negligible in large-scale computations, this fixed cost becomes a critical bottleneck for small-scale tasks. When the data scale surpasses 10^5, the overhead of memory copy rises rapidly, with a growth rate higher than those of kernel execution and synchronization processes. At a data scale of 10^8, memory copy accounts for approximately 50% of the total time and exhibits a tendency for further increase. Under this condition, the time contributions of memory allocation, kernel execution, and synchronization are approximately 14%, 18%, and 18%, respectively. The rapid escalation of memory copy overhead underscores the limitations of host-device data transfer bandwidth. The growth rate of memory copy time implies that the data transfer between the CPU and GPU becomes one of the primary factors influencing the computational performance of programs in heterogeneous cluster environments, and the I/O-bound workloads often underutilize GPU compute capabilities. Future efforts could focus on reducing communication overhead through strategies such as unified memory architecture and asynchronous communication. Additionally, integrating mixed-precision methods (Váňa et al., 2017), converting variables with minimal impact on simulation results from double-precision to single-precision, could further enhance data transfer efficiency between CPUs and GPUs.

https://doi.org/10.5194/egusphere-2026-3368
Preprint. Discussion started: 29 June 2026

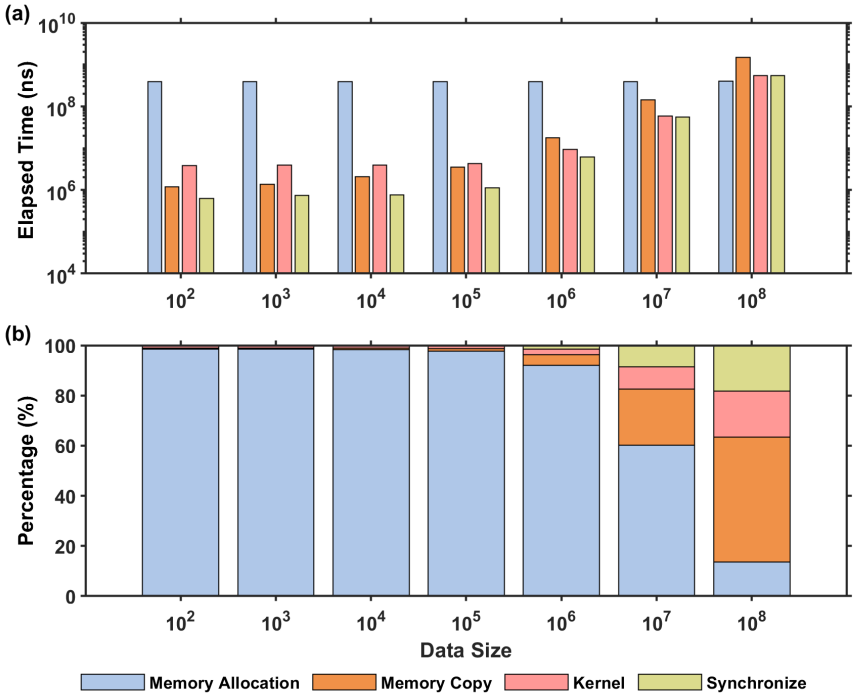

Figure 11. Time consumption **(a)** and proportional contributions **(b)** for memory allocation, memory copy, kernel, and synchronize process under the -O0 compilation flag and varying data scales.

4.3.2. Coupling performance comparison

Following the integration of GPU-HADVPPM4HIP V1.0 into the EPICC-Model V1.6.0, computational efficiency on the EarthLab was improved through communication optimization described in Sect. 3.2 and enhanced thread and block collaborative indexing detailed in Sect. 3.3. Furthermore, the hybrid parallelization scheme outlined in Sect. 3.4 was employed to extend the parallel computing scalability of the EPICC-Model V1.6.0 on the EarthLab. As introduced in Sect. 3.1, three model versions were established: the baseline unoptimized version HIP-Ori, the communication-optimized version HIP-Opt1, and the collaboratively indexed version HIP-Opt2 Figure 12(a) displays the average elapsed time required for a 28-hour simulation across these three versions. To ensure comparability, all tests adopted identical hardware configurations, including the MPI+HIP hybrid parallelization scheme with 10 CPU processes and 10 GPU-like accelerators, and were compiled using the -O3 optimization flag.

The GPU-HADVPPM4HIP V1.0 module features triple nested loops, and each invocation by

https://doi.org/10.5194/egusphere-2026-3368
Preprint. Discussion started: 29 June 2026

the EPICC-Model V1.6.0 necessitates data transfer between the CPU and GPU-like. Frequent CPU-GPU data transfer severely compromised the computational efficiency of the EPICC-Model V1.6.0 on the EarthLab. In the HIP-Ori unoptimized version, completing a 28-hour simulation required 149.7 hours, with an average hourly elapsed time of 19,241.0 seconds, equivalent to approximately 5.3 hours, reflecting critically low efficiency. After implementing communication optimizations in the HIP-Opt1 version, the communication frequency between the CPU and GPU-like was reduced from roughly 9.8 million to 10. This optimization drastically decreased the total elapsed time from 149.7 hours for HIP-Ori to 8.8 hours for HIP-Opt1, while the average hourly elapsed time dropped from 19,241.0 seconds to 1,133.7 seconds, achieving a 17.0x improvement in computational efficiency. Subsequently, collaborative indexing of threads and blocks was applied to parallelize the two-dimensional grid computations in the EPICC-Model V1.6.0. Compared to HIP-Opt1, the HIP-Opt2 version further reduced the total elapsed time from 8.8 hours to 6.0 hours, with the average hourly elapsed time decreasing from 1,133.7 seconds to 768.6 seconds. This enhancement delivered an additional 1.5x efficiency gain. Cumulatively, these optimizations elevated the computational efficiency of the EPICC-Model V1.6.0 on the EarthLab by approximately 25.0x.

By significantly improving the computational efficiency of the model on heterogeneous clusters through reducing the communication frequency between the CPU and GPU, we aim to emphasize the fundamental architectural differences between CPUs and GPUs. In recent years, although the substantial increase in GPU computational performance has opened up new directions for enhancing the efficiency of numerical models, the historical development of modeling frameworks means that early numerical models were predominantly designed for CPU architectures. Achieving parallel computation of numerical models on GPUs cannot be accomplished merely through straightforward code translation or by relying solely on heterogeneous programming interfaces. Instead, beyond adapting the model to GPUs, it is necessary to redesign the computational workflow, loop structures, and logical organization in accordance with GPU architectural characteristics, so as to fully leverage the powerful parallel computing capabilities of GPUs.

Figure 12(b) further compares the computational performance between the original Fortran-based version and the HIP-Opt2 version. In the figure, the label Fortran refers to the legacy CPU

https://doi.org/10.5194/egusphere-2026-3368
Preprint. Discussion started: 29 June 2026

cluster implementation of the EPICC-Model V1.6.0, while HIP represents the HIP-Opt2 version. Following the parallelization of the advection module on GPU-like accelerators, the EPICC-Model V1.6.0 demonstrated superior computational efficiency on heterogeneous clusters compared to its Fortran counterpart on conventional CPU clusters. The total elapsed time for a 28-hour simulation decreased from 2,287.4 seconds for the Fortran version to 2,152.0 seconds for the HIP version, with the average hourly elapsed time reduced from 817.0 seconds to 768.6 seconds.

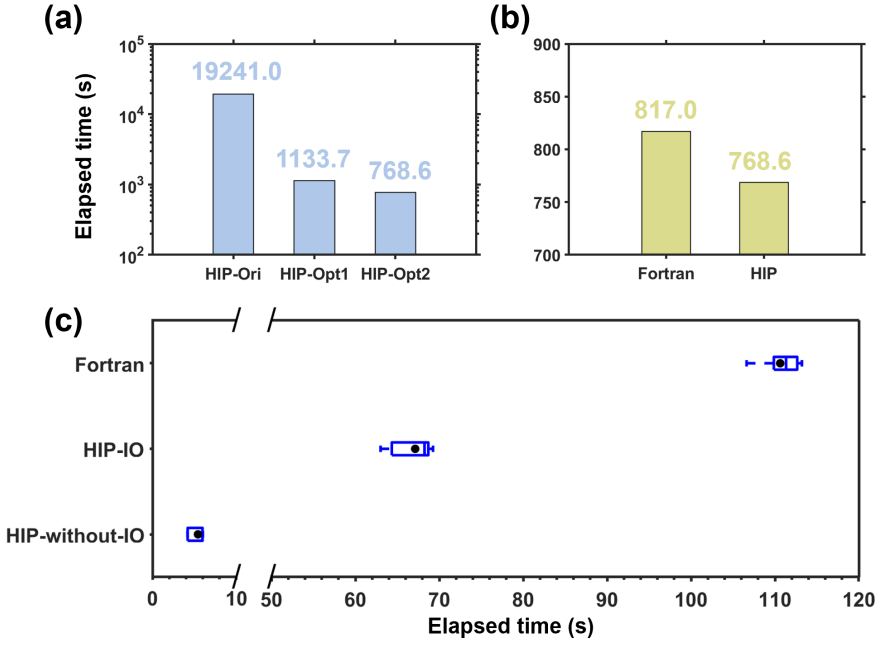

Figure 12. (a) The average hourly elapsed time required for a 28-hour simulation across HIP-Ori, HIP-Opt1, Opt2 versions; **(b)** the average hourly elapsed time required for a 28-hour simulation between the Fortran and HIP-Opt2 versions; **(c)** the hourly elapsed time required for a 28-hour simulation across the original Fortran-based HADVPPM program on CPUs, the GPU-HADVPPM4HIP V1.0 with CPU-GPU data transfer, and the GPU-HADVPPM4HIP V1.0 without data transfer. The black dots represent the average values, and the unit is seconds (s).

As demonstrated by the timing analysis of key processes in Sect. 4.3.1 for the offline heterogeneous computation of GPU-HADVPPM4HIP V1.0 on GPU-like accelerators, memory copying, specifically data transfer between the CPU and GPU, emerges as the dominant factor influencing parallel computational efficiency on heterogeneous clusters when handling large-scale

https://doi.org/10.5194/egusphere-2026-3368
Preprint. Discussion started: 29 June 2026

datasets. This overhead surpasses the time spent on kernel function parallelization. To quantify this effect, the computational time of GPU-HADVPPM4HIP V1.0 was separately evaluated on GPU-like accelerators under two scenarios: (1) including CPU-GPU data transfer and (2) excluding data transfer (kernel-only computation). In Figure 12 (c), the y-axis labels Fortran, HIP-IO, and HIP-without-IO correspond to the computational time of the original Fortran-based HADVPPM module on CPUs, the GPU-HADVPPM4HIP V1.0 with CPU-GPU data transfer on GPU-like accelerators, and the GPU-HADVPPM4HIP V1.0 without data transfer on GPU-like accelerators, respectively. All tests were compiled with the -O3 optimization flag, and timing metrics were averaged over a 28-hour simulation, focusing on the hourly computational cost of the advection module.

The original Fortran-based advection module required an average of 110.6 seconds per simulated hour on CPUs. After heterogeneous porting and parallel optimization to GPU-like accelerators, the GPU-HADVPPM4HIP V1.0 with data transfer achieved an average time of 67.1 seconds per simulation hour, representing a 39.3% improvement in computational efficiency. When excluding data transfer, the kernel-only GPU-HADVPPM4HIP V1.0 reduced the average time to 5.4 seconds per simulation hour, achieving a 20.5x acceleration compared to the Fortran version. These results underscore that while GPU-like accelerators deliver substantial computational power, the efficiency of CPU-GPU data transfer critically constrains overall performance on heterogeneous clusters. To mitigate this bottleneck, future work will focus on retaining I/O operations on CPUs while porting the entire physicochemical integration module (excluding I/O) to GPUs for parallel computation. This strategy is expected to reduce the impact of inter-device data transfer and further enhance scalability.

5. Conclusions and discussion

In recent years, the rapid advancement in the computational performance of GPUs has provided novel approaches and hardware foundations for improving the computational efficiency of air quality models. Building upon the heterogeneous porting and parallel optimization technology system for air quality model, this study further implements parallel computing of the advection module in the EPICC-Model air quality modeling system on GPU-like accelerators, validating the feasibility of the heterogeneous porting framework. The study involves three key technical

https://doi.org/10.5194/egusphere-2026-3368
Preprint. Discussion started: 29 June 2026

699 improvements. The first is restructuring the original Fortran code of the advection module using
700 standard C language programming. The second is porting the advection module to GPU-like
701 accelerators through HIP heterogeneous programming technology, in addition, computational
702 efficiency was enhanced through optimizing CPU-GPU data transfer frequency reduction,
703 coordinated indexing of threads and blocks, and hybrid parallelization strategies. These
704 optimizations collectively improved both the computational performance of the advection module
705 and the parallel computing scalability of the EPICC-Model V1.6.0 on the EarthLab.

706 This study systematically conducted comparative efficiency analyses by the validation of
707 computational consistency in GPU-HADVPPM4HIP V1.0 through offline testing methodologies,
708 as well as the verification of EPICC-Model's pollutant simulation performance on the EarthLab.
709 Initial benchmarking compared the offline computational efficiency between the original Fortran-
710 based HADVPPM program on domestic CPUs and the GPU-HADVPPM4HIP V1.0
711 implementation. The results demonstrated that the -O3 compiler optimization flag significantly
712 enhanced GPU-HADVPPM4HIP's computational efficiency, with acceleration effects becoming
713 more pronounced at larger data scales. Specifically, at 10^8 data size configuration, GPU-
714 HADVPPM4HIP V1.0 achieved a maximum 556.5x speedup over the Fortran baseline using default
715 -O0 compilation, while maintaining a 128.0x speedup advantage even when both implementations
716 employed -O3 optimization. Further profiling of GPU-HADVPPM4HIP's heterogeneous
717 computation on GPU-like accelerators revealed critical characteristics: Memory copy operations
718 (i.e., CPU-GPU data transfers) exhibited elapsed time increases rapidly with data size increasing,
719 accounting for approximately 50% of total computation time at 10^8 data size with a continuing
720 upward trend. This observation underscores data transfer efficiency as a critical bottleneck for high-
721 resolution air quality simulations in heterogeneous computing environments.

722 Coupling GPU-HADVPPM4HIP V1.0 into EPICC-Model V1.6.0 with data transfer
723 optimizations and thread-block coordinated indexing strategies yielded system-level performance
724 improvements of 17.0x and 1.5x respectively on the EarthLab. The detailed module-level analysis
725 demonstrated that GPU-HADVPPM4HIP V1.0 achieved 39.3% efficiency enhancement over the
726 original Fortran advection module when accounting for CPU-GPU data transfer overheads,
727 escalating to a 20.5x acceleration when excluding data transfer costs. These findings quantitatively

https://doi.org/10.5194/egusphere-2026-3368
Preprint. Discussion started: 29 June 2026

validate the substantial impact of CPU-GPU data transfer efficiency on the operational performance of air quality models in heterogeneous computing architectures.

There remains considerable room for improving the computational performance of GPU-HADVPPM4HIP V1.0 within the EPICC-Model in this study. First, constrained by the thermal dissipation limits of transistors, the growth in computational performance of CPU processors has slowed and is gradually approaching its physical limits. In recent years, however, GPU processors have continued to achieve substantial performance gains due to their architectural advantages, and heterogeneous supercomputing architectures centered on "CPU+GPU" now dominate the landscape of advanced high-performance computing systems worldwide. Taking the 66th TOP500 list released in November 2025 as an example, 9 out of the top 10 supercomputers adopt heterogeneous architectures. Hence, heterogeneous computing represents the primary direction for the future development of supercomputing. That said, the advancement of numerical models relies fundamentally on the support of supercomputing capabilities. The team awarded the Gordon Bell Prize for Climate Modeling in November 2025 leveraged the powerful computational capacity of NVIDIA GH200 GPUs to accomplish the world's first 1.25 km ultra-high-resolution Earth system simulation (Klocke et al., 2025). To achieve kilometer-scale, ultra-high-resolution simulations of atmospheric pollution, it is both essential and imperative to adapt air quality models to heterogeneous supercomputing environments and enable efficient parallel computing.

Moreover, results from offline computational performance tests in this study and coupled performance tests in Cao et al. (2024) consistently show that the acceleration effect of GPUs becomes more pronounced as the computational scale increases, which sufficiently demonstrates the potential of GPUs in large-scale, high-resolution application scenarios. The simulation case configured in this study, with a resolution of only 15 km over the whole of China, may not yet fully reflect the parallel computing advantages of GPUs. In the future, higher-resolution simulation cases will be designed to better highlight the performance advantages of GPU acceleration.

Finally, in future work, we will employ further optimization techniques to enhance the computational performance of the advection module and other computationally intensive modules in the EPICC-Model on domestic heterogeneous clusters, including but not limited to:

(1) Firstly, priority should be given to optimizing CPU-GPU data transfer efficiency by reducing

https://doi.org/10.5194/egusphere-2026-3368
Preprint. Discussion started: 29 June 2026

communication overhead through strategies such as unified memory architecture, asynchronous communication, mixed-precision methods, and minimizing non-essential variable I/O in air quality forecasting.

(2) Second, while GPU-accelerated modules including the gas-phase chemistry module (Cao et al., 2025) and advection module have been individually developed, their systematic integration into EPICC-Model requires architectural refinement to increase GPU code coverage. We will analyze the computational characteristics of the code in other modules of the model. For code segments involving iterative computations, we will first decouple the iterative computations by creating intermediate variables, thereby eliminating dependencies between successive calculation steps. Subsequently, the computational code of other modules after iterative decoupling will be rewritten in the form of Kernel functions to increase the proportion of code executed on the GPU.

(3) Finally, in current heterogeneous architecture supercomputing systems, the number of CPU processes within a computing node typically exceeds the number of GPUs. Employing the current matching scheme of one CPU process to one GPU accelerator results in the waste of remaining CPU computing resources. In the future, on one hand, while avoiding data transmission competition between the CPU and GPU, we will consider designing a more sophisticated mechanism for matching multiple CPU processes with a single GPU. On the other hand, drawing on Cao et al. (2024), we plan to introduce an OpenMP shared-memory parallel scheme into the EPICC-Model. Through multi-level hybrid parallelism, while porting computationally intensive modules to the GPU for parallel computing, other modules running on the CPU will utilize OpenMP multithreading parallelism, thereby fully leveraging CPU computing resources.

Consequently, achieving efficient parallel computation of air quality models on GPU accelerators necessitates collaboration between researchers well-versed in the intrinsic physicochemical mechanisms of the models and engineers with expertise in GPU hardware and software. Herein, we appeal for the participation of engineers specializing in GPU software and hardware development to jointly advance the progress of air quality modeling.

https://doi.org/10.5194/egusphere-2026-3368
Preprint. Discussion started: 29 June 2026

Code and data availability. The source codes of EPICC-Model V1.6.0 are available online via ZENODO (https://zenodo.org/records/20303367, EPICC-Model Working Group, 2026). The GPU acceleration code of HADVPPM scheme in the EPICC-Model, datasets, and the offline test code related to this paper are available online via ZENODO (https://zenodo.org/records/20605319, Cao et al., 2026).

Author contributions. KC and QW refactored the existing code, visualization, and prepared the materials. QW, XT, JZ, and ZW planned and organized the project. KC, QW, JinL, XC, HC, WW, and LK optimized the GPU-based codes. HC, WW, HW, and JieL prepared the data and conducted the simulation. KC, QW, TX, XC, WW, JieL, JZ, and ZW carried out formal analysis of the model results. KC, QW, TX, JinxL, XC, HC, WW, LK, and ZW took part in the discussion.

Competing interests. The authors declare that they have no conflict of interest.

Acknowledgements. The Strategic Priority Research Program of the Chinese Academy of Sciences (grant no. XDB0760401), the National Key Research and Development Program of China (grant no. 2023YFC3705705), the State Key Laboratory of Atmospheric Environment and Extreme Meteorology (grant no. 2024QN08), the National Natural Science Foundation of China (grant nos. 42507147 and 42377105), and the Key Research and Development Program of Henan Province (grant no. 241111212300) funded this work. The authors would like to thank for the technical support of the National large Scientific and Technological Infrastructure "Earth System Numerical Simulation Facility" (https://cstr.cn/31134.02.EL).

Financial support. This research has been supported by the Strategic Priority Research Program of the Chinese Academy of Sciences (grant no. XDB0760401), the National Key Research and

https://doi.org/10.5194/egusphere-2026-3368
Preprint. Discussion started: 29 June 2026

Development Program of China (grant no. 2023YFC3705705), the State Key Laboratory of Atmospheric Environment and Extreme Meteorology (grant no. 2024QN08), and the National Natural Science Foundation of China (grant nos. 42507147 and 42377105).

Reference

Adani, M., D'Isidoro, M., Mircea, M., Guarnieri, G., Vitali, L., D'Elia, I., Ciancarella, L., Gualtieri, M., Briganti, G., Cappelletti, A., Piersanti, A., Stracquadanio, M., Righini, G., Russo, F., Cremona, G., Villani, M. G., and Zanini, G.: Evaluation of air quality forecasting system FORAIR-IT over Europe and Italy at high resolution for year 2017, Atmos. Pollut. Res., 13, 10.1016/j.apr.2022.101456, 2022.

Alvanos, M. and Christoudias, T.: GPU-accelerated atmospheric chemical kinetics in the ECHAM/MESSy (EMAC) Earth system model (version 2.52), Geosci. Model Dev., 10, 3679-3693, 10.5194/gmd-10-3679-2017, 2017.

AMD: ROCm Documentation Release 5.7.1, Advanced Micro Devices Inc., https://rocm.docs.amd.com/en/docs-5.7.1/ (last access: 26 May 2025), 2023.

Appel, K. W., Bash, J. O., Fahey, K. M., Foley, K. M., Gilliam, R. C., Hogrefe, C., Hutzell, W. T., Kang, D., Mathur, R., Murphy, B. N., Napelenok, S. L., Nolte, C. G., Pleim, J. E., Pouliot, G. A., Pye, H. O. T., Ran, L., Roselle, S. J., Sarwar, G., Schwede, D. B., Sidi, F. I., Spero, T. L., and Wong, D. C.: The Community Multiscale Air Quality (CMAQ) model versions 5.3 and 5.3.1: system updates and evaluation, Geosci. Model Dev., 14, 2867-2897, 10.5194/gmd-14-2867-2021, 2021.

Atkinson, R. W., Fuller, G. W., Anderson, H. R., Harrison, R. M., and Armstrong, B.: Urban ambient particle metrics and health: a time-series analysis, Epidemiology (Cambridge, Mass.), 21, 501-511, 10.1097/EDE.0b013e3181debc88, 2010.

Byun, D. W. and Dennis, R.: Design artifacts in eulerian air quality models: Evaluation of the effects of layer thickness and vertical profile correction on surface ozone concentrations, Atmos. Environ., 29, 105-126, https://doi.org/10.1016/1352-2310(94)00225-A, 1995.

Cao, K., Wu, Q., and Tang, Xiao.: The dataset of the manuscript "Enhancing the advection module performance in the EPICC-Model V1.6.0 via GPU-HADVPPM4HIP V1.0 coupling and GPU-

https://doi.org/10.5194/egusphere-2026-3368
Preprint. Discussion started: 29 June 2026

optimized strategies", Zenodo [data set], https://doi.org/10.5281/zenodo.20605319, 2026.

Cao, K., Wu, Q., Wang, L., Wang, N., Cheng, H., Tang, X., Li, D., and Wang, L.: GPU-HADVPPM V1.0: a high-efficiency parallel GPU design of the piecewise parabolic method (PPM) for horizontal advection in an air quality model (CAMx V6.10), Geosci. Model Dev., 16, 4367-4383, 10.5194/gmd-16-4367-2023, 2023.

Cao, K., Wu, Q., Wang, L., Guo, H., Wang, N., Cheng, H., Tang, X., Li, D., Liu, L., Li, D., Wu, H., and Wang, L.: GPU-HADVPPM4HIP V1.0: using the heterogeneous-compute interface for portability (HIP) to speed up the piecewise parabolic method in the CAMx (v6.10) air quality model on China's domestic GPU-like accelerator, Geosci. Model Dev., 17, 6887-6901, 10.5194/gmd-17-6887-2024, 2024.

Cao, K., Tang, X., Chen, H., Ma, J., Wu, Q., Wang, W., Chen, X., Li J., Wang, Z.: Porting and Parallel Optimization of the Gas-phase Chemistry Module of the Air Quality Model EPICC-Model on China’s Domestic Accelerators, Frontiers of Data&Computing, 10.11871/jfdc.issn.2096-742X.2025.05.010, 2025 (in Chinese).

Chai, Z., Zhang, H., Zhang, M., Tang, X., Zheng, W., Zhu, J., Zhou, G., Cao, J., and Zeng, Q.: China’s EarthLab—Forefront of Earth System Simulation Research, Adv. Atmos. Sci., 38, 1611-1620, 10.1007/s00376-021-1175-y, 2021.

Chang, J. S., Brost, R. A., Isaksen, I. S. A., Madronich, S., Middleton, P., Stockwell, W. R., and Walcek, C. J.: A three-dimensional Eulerian acid deposition model: Physical concepts and formulation, J. Geophys. Res.-Atmos., 92, 14681-14700, https://doi.org/10.1029/JD092iD12p14681, 1987.

Colella, P. and Woodward, P. R.: The Piecewise Parabolic Method (PPM) for gas-dynamical simulations, J. Comput. Phys., 54, 174-201, https://doi.org/10.1016/0021-9991(84)90143-8, 1984.

Crippa, M., Guizzardi, D., Pagani, F., Schiavina, M., Melchiorri, M., Pisoni, E., Graziosi, F., Muntean, M., Maes, J., Dijkstra, L., Van Damme, M., Clarisse, L., and Coheur, P.: Insights into the spatial distribution of global, national, and subnational greenhouse gas emissions in the Emissions Database for Global Atmospheric Research (EDGAR v8.0), Earth Syst. Sci. Data, 16, 2811-2830, 10.5194/essd-16-2811-2024, 2024.

https://doi.org/10.5194/egusphere-2026-3368
Preprint. Discussion started: 29 June 2026

872 Crippa, M., Guizzardi, D., Butler, T., Keating, T., Wu, R., Kaminski, J., Kuenen, J., Kurokawa, J.,
873 Chatani, S., Morikawa, T., Pouliot, G., Racine, J., Moran, M. D., Klimont, Z., Manseau, P. M.,
874 Mashayekhi, R., Henderson, B. H., Smith, S. J., Suchyta, H., Muntean, M., Solazzo, E., Banja,
875 M., Schaaf, E., Pagani, F., Woo, J. H., Kim, J., Monforti-Ferrario, F., Pisoni, E., Zhang, J.,
876 Niemi, D., Sassi, M., Ansari, T., and Foley, K.: The HTAP_v3 emission mosaic: merging
877 regional and global monthly emissions (2000–2018) to support air quality modelling and
878 policies, Earth Syst. Sci. Data, 15, 2667-2694, 10.5194/essd-15-2667-2023, 2023.
879 Damian, V., Sandu, A., Damian, M., Potra, F., and Carmichael, G. R.: The kinetic preprocessor KPP-
880 a software environment for solving chemical kinetics, Comput. Chem. Eng., 26, 1567-1579,
881 https://doi.org/10.1016/S0098-1354(02)00128-X, 2002.
882 Elbern, H.: Parallelization and load balancing of a comprehensive atmospheric chemistry transport
883 model, Atmos. Environ., 31, 3561-3574, https://doi.org/10.1016/S1352-2310(97)00157-
884 X,1997.
885 Emery, C., Baker, K., Wilson, G., and Yarwood, G.: Comprehensive Air Quality Model with
886 Extensions: Formulation and Evaluation for Ozone and Particulate Matter over the US,
887 Atmosphere, 15, 1158. https://doi.org/10.3390/atmos15101158, 2024.
888 EPICC-Model Working Group.: Description and evaluation of the Emission and atmospheric
889 Processes Integrated and Coupled Community (EPICC) Model version 1.0. Adv. Atmos. Sci.,
890 http://www.iapjournals.ac.cn/aas/en/article/doi/10.1007/s00376-025-4384-y, 2025.
891 EPICC-Model Working Group. : Emission and atmospheric Processes Integrated and Coupled
892 Community Model (EPICC-Model). Zenodo. https://doi.org/10.5281/zenodo.20303367, 2026.
893 Gao, Z. and Zhou, X.: A review of the CAMx, CMAQ, WRF-Chem and NAQPMS models:
894 Application, evaluation and uncertainty factors, Environ. Pollut., 343,
895 10.1016/j.envpol.2023.123183, 2024.
896 Georgiou, G. K., Christoudias, T., Proestos, Y., Kushta, J., Hadjinicolaou, P., and Lelieveld, J.: Air
897 quality modelling in the summer over the eastern Mediterranean using WRF-Chem: chemistry
898 and aerosol mechanism intercomparison, Atmos. Chem. Phys., 18, 1555-1571, 10.5194/acp-
899 18-1555-2018, 2018.
900 Georgiou, G. K., Christoudias, T., Proestos, Y., Kushta, J., Pikridas, M., Sciare, J., Savvides, C., and

https://doi.org/10.5194/egusphere-2026-3368
Preprint. Discussion started: 29 June 2026

Lelieveld, J.: Evaluation of WRF-Chem model (v3.9.1.1) real-time air quality forecasts over the Eastern Mediterranean, Geosci. Model Dev., 15, 4129-4146, 10.5194/gmd-15-4129-2022, 2022.

Guevara, M., Jorba, O., Tena, C., Denier van der Gon, H., Kuenen, J., Elguindi, N., Darras, S., Granier, C., and Pérez García-Pando, C.: Copernicus Atmosphere Monitoring Service TEMPOral profiles (CAMS-TEMPO): global and European emission temporal profile maps for atmospheric chemistry modelling, Earth Syst. Sci. Data, 13, 367-404, 10.5194/essd-13-367-2021, 2021.

Gupta, M. and Mohan, M.: Validation of WRF/Chem model and sensitivity of chemical mechanisms to ozone simulation over megacity Delhi, Atmos. Environ., 122, 220-229, 10.1016/j.atmosenv.2015.09.039, 2015.

Hong, S.-Y., Noh, Y., and Dudhia, J.: A New Vertical Diffusion Package with an Explicit Treatment of Entrainment Processes, Mon. Weather Rev., 134, 2318-2341, https://doi.org/10.1175/MWR3199.1, 2006.

Intel Software: Quick Reference Guide to Optimization with Intel C++ and Fortran Compilers v19, Intel, https://www.intel.cn/content/www/cn/zh/developer/articles/technical/intel-fortran-and-c-compiler-documentation.html. (last access: 26 May 2025), 2020.

Kim, K.-H., Kabir, E., and Kabir, S.: A review on the human health impact of airborne particulate matter, Environ. Int., 74, 136-143, https://doi.org/10.1016/j.envint.2014.10.005, 2015.

Klocke, D., Frauen, C., Engels, J. F., Alexeev, D., Redler, R., Schnur, R., Haak, H., Kornblueh, L., Brüggemann, N., Chegini, F., Römmer, M., Hoffmann, L., Griessbach, S., Bode, M., Coles, J., Gila, M., Sawyer, W., Calotoiu, A., Budanaz, Y., Mazumder, P., Copik, M., Weber, B., Herten, A., Bockelmann, H., Hoefler, T., Hohenegger, C., and Stevens, B.: Computing the Full Earth System at 1km Resolution, Proceedings of the International Conference for High Performance Computing, Networking, Storage and Analysis, 10.1145/3712285.3771789, 2025.

Kong, L., Tang, X., Wang, Z., Zhu, J., Li, J., Wu, H., Wu, Q., Chen, H., Zhu, L., Wang, W., Liu, B., Wang, Q., Chen, D., Pan, Y., Li, J., Wu, L., and Carmichael, G. R.: Changes in air pollutant emissions in China during two clean-air action periods derived from the newly developed Inversed Emission Inventory for Chinese Air Quality (CAQIEI), Earth Syst. Sci. Data, 16,

https://doi.org/10.5194/egusphere-2026-3368
Preprint. Discussion started: 29 June 2026

4351-4387, 10.5194/essd-16-4351-2024, 2024.

Li, J., Wang, Z., Zhuang, G., Luo, G., Sun, Y., and Wang, Q.: Mixing of Asian mineral dust with anthropogenic pollutants over East Asia: a model case study of a super-duststorm in March 2010, Atmos. Chem. Phys., 12, 7591-7607, 10.5194/acp-12-7591-2012, 2012.

Li, J., Chen, X., Wang, Z., Du, H., Yang, W., Sun, Y., Hu, B., Li, J., Wang, W., Wang, T., Fu, P., and Huang, H.: Radiative and heterogeneous chemical effects of aerosols on ozone and inorganic aerosols over East Asia, Sci. Total Environ., 622-623, 1327-1342, https://doi.org/10.1016/j.scitotenv.2017.12.041, 2018.

Li, M., Liu, H., Geng, G., Hong, C., Liu, F., Song, Y., Tong, D., Zheng, B., Cui, H., Man, H., Zhang, Q., and He, K.: Anthropogenic emission inventories in China: a review, Natl. Sci. Rev., 4, 834-866, 10.1093/nsr/nwx150, 2017.

Linford, J. C., Michalakes, J., Vachharajani, M., and Sandu, A.: Automatic Generation of Multicore Chemical Kernels, IEEE T. Parall. Distr., 22, 119-131, 10.1109/tpds.2010.106, 2011.

Liu, J., Han, Y., Tang, X., Zhu, J., and Zhu, T.: Estimating adult mortality attributable to PM2.5 exposure in China with assimilated PM2.5 concentrations based on a ground monitoring network, Sci. Total. Environ., 568, 1253-1262, https://doi.org/10.1016/j.scitotenv.2016.05.165, 2016.

Milton, L. A. and White, A. R.: The potential impact of bushfire smoke on brain health, Neurochem. Int., 139, 104796, 10.1016/j.neuint.2020.104796, 2020.

NVIDIA: CUDA C++ Programming Guide Version 10.2, NVIDIA Corporation, https://docs.nvidia.com/cuda/archive/10.2/pdf/CUDA_C_Programming_Guide.pdf (last access: 26 May 2025), 2020.

Nenes, A., Pandis, S. N., and Pilinis, C.: ISORROPIA: A New Thermodynamic Equilibrium Model for Multiphase Multicomponent Inorganic Aerosols, Aquat. Geochem., 4, 123-152, 10.1023/A:1009604003981, 1998.

Podrascanin, Z.: Setting-up a Real-Time Air Quality Forecasting system for Serbia: a WRF-Chem feasibility study with different horizontal resolutions and emission inventories, Environ. Sci. Pollut. R., 26, 17066-17079, 10.1007/s11356-019-05140-y, 2019.

Quevedo, D., Do, K., Delic, G., Rodríguez-Borbón, J., Wong, B. M., and Ivey, C. E.: GPU

https://doi.org/10.5194/egusphere-2026-3368
Preprint. Discussion started: 29 June 2026

Implementation of a Gas-Phase Chemistry Solver in the CMAQ Chemical Transport Model, ACS ES&T Air, 2, 226-235, 10.1021/acsestair.4c00181, 2025.

Sandu, A., Verwer, J. G., Van Loon, M., Carmichael, G. R., Potra, F. A., Dabdub, D., and Seinfeld, J. H.: Benchmarking stiff ode solvers for atmospheric chemistry problems-I. implicit vs explicit, Atmos. Environ., 31, 3151-3166, https://doi.org/10.1016/S1352-2310(97)00059-9, 1997.

Skamarock, W. C., Klemp, J. B., Dudhia, J., Gill, D. O., Barker, D.M., Duda, M. G., Huang, X. Y., Wang, W., and Powers, J. G.: A Description of the Advanced Research WRF Version3 (No.NCAR/TN-475CSTR), University Corporation for Atmospheric Research, NCAR, https://doi.org/10.5065/D68S4MVH, 2008.

Sun, J., Fu, J. S., Drake, J. B., Zhu, Q., Haidar, A., Gates, M., Tomov, S., and Dongarra, J.: Computational Benefit of GPU Optimization for the Atmospheric Chemistry Modeling, J. Adv. Model. Earth. Sy., 10, 1952-1969, https://doi.org/10.1029/2018MS001276, 2018.

Tang, Y., Campbell, P. C., Lee, P., Saylor, R., Yang, F., Baker, B., Tong, D., Stein, A., Huang, J., Huang, H.-C., Pan, L., McQueen, J., Stajner, I., Tirado-Delgado, J., Jung, Y., Yang, M., Bourgeois, I., Peischl, J., Ryerson, T., Blake, D., Schwarz, J., Jimenez, J.-L., Crawford, J., Diskin, G., Moore, R., Hair, J., Huey, G., Rollins, A., Dibb, J., and Zhang, X.: Evaluation of the NAQFC driven by the NOAA Global Forecast System (version 16): comparison with the WRF-CMAQ during the summer 2019 FIREX-AQ campaign, Geosci. Model Dev., 15, 7977-7999, 10.5194/gmd-15-7977-2022, 2022.

Thompson, T. M. and Selin, N. E.: Influence of air quality model resolution on uncertainty associated with health impacts, Atmos. Chem. Phys., 12, 9753-9762, 10.5194/acp-12-9753-2012, 2012.

Top500: Supercomputing Top500 list, TOP500 international organization, https://www.top500.org/lists/top500/2024/11/ (last access: 26 May 2025), 2024.

Váňa, F., Düben, P., Lang, S., Palmer, T., Leutbecher, M., Salmond, D., and Carver, G.: Single Precision in Weather Forecasting Models: An Evaluation with the IFS, Mon. Weather Rev., 145, 495–502, https://doi.org/10.1175/mwr-d-16-0228.1, 2017.

Walcek, C. J. and Aleksic, N. M.: A simple but accurate mass conservative, peak-preserving, mixing ratio bounded advection algorithm with FORTRAN code, Atmos. Environ., 32, 3863-3880,

https://doi.org/10.5194/egusphere-2026-3368
Preprint. Discussion started: 29 June 2026

https://doi.org/10.1016/S1352-2310(98)00099-5, 1998.

Wang, H., Chen, H., Wu, Q., Lin, J., Chen, X., Xie, X., Wang, R., Tang, X., and Wang, Z.: GNAQPMS v1.1: accelerating the Global Nested Air Quality Prediction Modeling System (GNAQPMS) on Intel Xeon Phi processors, Geosci. Model Dev., 10, 2891-2904, 10.5194/gmd-10-2891-2017, 2017.

Wang, H., Lin, J., Wu, Q., Chen, H., Tang, X., Wang, Z., Chen, X., Cheng, H., and Wang, L.: MP CBM-Z V1.0: design for a new Carbon Bond Mechanism Z (CBM-Z) gas-phase chemical mechanism architecture for next-generation processors, Geosci. Model Dev., 12, 749-764, 10.5194/gmd-12-749-2019, 2019.

Wang, P., Jiang, J., Lin, P., Ding, M., Wei, J., Zhang, F., Zhao, L., Li, Y., Yu, Z., Zheng, W., Yu, Y., Chi, X., and Liu, H.: The GPU version of LASG/IAP Climate System Ocean Model version 3 (LICOM3) under the heterogeneous-compute interface for portability (HIP) framework and its large-scale application, Geosci.Model Dev., 14, 2781–2799, https://doi.org/10.5194/gmd-14-2781-2021, 2021.

Wang, W., Chen, H., Wang, Z., Li, J., Chen, X., Yu, F., Fan, X., Zhao, S., Hu, B., Wang, W., Tang, X., Wang, Z., Ge, B., and Wu, J.: Development and evaluation of photolysis and gas-phase reaction scheme in EPICC-model: Impacts on tropospheric ozone simulation, Atmos. Environ., 359, https://doi.org/10.1016/j.atmosenv.2025.121373, 2025.

Wesely, M. L.: Parameterization of surface resistances to gaseous dry deposition in regional-scale numerical models, Atmos. Environ.(1967), 23, 1293-1304, https://doi.org/10.1016/0004-6981(89)90153-4, 1989.

Wu, H., Tang, X., Wang, Z., Wu, L., Lu, M., Wei, L., and Zhu, J.: Probabilistic Automatic Outlier Detection for Surface Air Quality Measurements from the China National Environmental Monitoring Network, Adv. Atmos. Sci., 35, 1522-1532, 10.1007/s00376-018-8067-9, 2018.

Wu, Q. Z., Xu, W. S., Shi, A. J., Li, Y. T., Zhao, X. J., Wang, Z. F., Li, J. X., and Wang, L. N.: Air quality forecast of PM_{10} in Beijing with Community Multi-scale Air Quality Modeling (CMAQ) system: emission and improvement, Geosci. Model Dev., 7, 2243-2259, 10.5194/gmd-7-2243-2014, 2014.

Yarwood, G., Shi, Y., Beardsley, R.: Impact of cb6r5 mechanism changes on air pollutant modeling

https://doi.org/10.5194/egusphere-2026-3368
Preprint. Discussion started: 29 June 2026

in Texas. Final report prepared for the Texas Commission on Environmental Quality, Austin, TX. https://www.tceq.texas.gov/airquality/airmod/project/pj_report_pm.html, 2020.

Yang, J., Qu, Y., Chen, Y., Zhang, J., Liu, X., Niu, H., and An, J.: Dominant physical and chemical processes impacting nitrate in Shandong of the North China Plain during winter haze events, Sci. Total Environ., 912, 169065, https://doi.org/10.1016/j.scitotenv.2023.169065, 2024.

Zaveri, R. A. and Peters, L. K.: A new lumped structure photochemical mechanism for large-scale applications, J. Geophys. Res.-Atmos., 104, 30387-30415, 10.1029/1999jd900876, 1999.

Zhang, J., Lian, C., Wang, W., Ge, M., Guo, Y., Ran, H., Zhang, Y., Zheng, F., Fan, X., Yan, C., Daellenbach, K. R., Liu, Y., Kulmala, M., and An, J.: Amplified role of potential HONO sources in O3 formation in North China Plain during autumn haze aggravating processes, Atmos. Chem. Phys., 22, 3275-3302, 10.5194/acp-22-3275-2022, 2022.

Zhang, L., Brook, J. R., and Vet, R.: A revised parameterization for gaseous dry deposition in air-quality models, Atmos. Chem. Phys., 3, 2067-2082, 10.5194/acp-3-2067-2003, 2003.

Zhu, T., Tang, M., Gao, M., Bi, X., Cao, J., Che, H., Chen, J., Ding, A., Fu, P., Gao, J., Gao, Y., Ge, M., Ge, X., Han, Z., He, H., Huang, R.-J., Huang, X., Liao, H., Liu, C., Liu, H., Liu, J., Liu, S. C., Lu, K., Ma, Q., Nie, W., Shao, M., Song, Y., Sun, Y., Tang, X., Wang, T., Wang, T., Wang, W., Wang, X., Wang, Z., Yin, Y., Zhang, Q., Zhang, W., Zhang, Y., Zhang, Y., Zhao, Y., Zheng, M., Zhu, B., and Zhu, J.: Recent Progress in Atmospheric Chemistry Research in China: Establishing a Theoretical Framework for the "Air Pollution Complex", Adv. Atmos. Sci., 40, 1339-1361, 10.1007/s00376-023-2379-0, 2023.